Atmos. Chem. Phys. Discuss., 10, 18661–18730, 2010
www.atmos-chem-phys-discuss.net/10/18661/2010/
doi:10.5194/acpd-10-18661-2010

Atmospheric Chemistry and Physics Discussions

Development and evaluation of the aerosol dynamic and gas phase chemistry model ADCHEM

P. Roldin[1], E. Swietlicki[1], G. Schurgers[2], A. Arneth[2], K. E. J. Lehtinen[3,4], M. Boy[5], and M. Kulmala[5]

[1]Division of Nuclear Physics, Lund University, 221 00, Lund, Sweden
[2]Department of Earth and Ecosystem Sciences, Lund University, Sweden
[3]Department of Physics and Mathematics, University of Eastern Finland, Kuopio, Finland
[4]Finnish Meteorological Institute, Kuopio Unit, Kuopio, Finland
[5]Atmospheric Sciences Division, Department of Physics, University of Helsinki, Finland

Received: 14 July 2010 – Accepted: 18 July 2010 – Published: 10 August 2010

Correspondence to: P. Roldin (pontus.roldin@nuclear.lu.se)

Published by Copernicus Publications on behalf of the European Geosciences Union.

Abstract

The aim of this work was to develop a model ideally suited for detailed studies on aerosol dynamics, gas and particle phase chemistry within urban plumes, from local scale ($1\times1\,km^2$) to regional or global scale. This article describes and evaluates the trajectory model for Aerosol Dynamics, gas and particle phase CHEMistry and radiative transfer (ADCHEM), which has been developed and used at Lund University since 2007. The model treats both vertical and horizontal dispersion perpendicular to an air mass trajectory (2-space dimensions), which is not treated in Lagrangian box-models (0-space dimensions). The Lagrangian approach enables a more detailed representation of the aerosol dynamics, gas and particle phase chemistry and a finer spatial and temporal resolution compared to that of available regional 3D-CTMs. These features make it among others ideally suited for urban plume studies. The aerosol dynamics model includes Brownian coagulation, dry deposition, wet deposition, in-cloud processing, condensation, evaporation, primary particle emissions and homogeneous nucleation. The gas phase chemistry model calculates the gas phase concentrations of 63 different species, using 119 different chemical reactions. Daily isoprene and monoterpene emissions from European forests were simulated separately with the vegetation model LPJ-GUESS, and included as input to ADCHEM. ADCHEM was used to simulate the ageing of the urban plumes from the city of Malmö in Southern Sweden (280 000 inhabitants). Several sensitivity tests were performed concerning the number of size bins, size structure method, coupled or uncoupled condensation, the volatility basis set (VBS) or traditional 2-product model for secondary organic aerosol formation, different aerosol dynamic processes and vertical and horizontal mixing. The simulations show that the full-stationary size structure gives accurate results with little numerical diffusion when more than 50 size bins are used between 1.5 and 2500 nm, while the moving-center method is preferable when only a few size bins are selected. The particle number size distribution in the center of the urban plume from Malmö is mainly affected by dry deposition, coagulation and condensation, and is relatively in-

ACPD

10, 18661–18730, 2010

sensitive to moderate variations in the vertical and horizontal mixing, as long as the mixing height is relatively uniform. The modeled $PM_{2.5}$ was dominated by organics, nitrate, sulfate and ammonium. If treating the condensation of HNO_3 and NH_3 as a coupled process (pH independent) the model gave lower nitrate $PM_{2.5}$ values than if considering uncoupled condensation. However, both methods gave similar and significant temporal variation in the particulate nitrate content, primarily due to fluctuation in the relative humidity.

1 Introduction and background

Since the chemical and physical properties of aerosol particles determine both their climate and health effects, it is important to understand the aerosol dynamic processes that affect these quantities. Particle emissions within a city may have a significant effect on the health and climate several tens or hundreds of kilometers downwind of the urban center, although limited quantitative information is available in the literature. The chemical composition of the ambient aerosols is affected by primary particle emissions, condensation, evaporation and coagulation between particles with different composition. The particle number size distribution is altered by emissions, condensation, evaporation, coagulation, dry and wet deposition, formation of new particles by homogeneous nucleation and in-cloud processing.

Since 2007 the trajectory model for Aerosol Dynamics, gas and particle phase CHEMistry and radiative transfer (ADCHEM) has continuously been developed and used at Lund University. ADCHEM was used to model the particle and gas phase properties in the urban plume from the city of Malmö in Southern Sweden (13°00′ E, 55°36′ N, 280 000 inhabitants). This article mainly describes the model development and evaluation, while Paper II (Roldin et al., 2010) describes the average particle and gas phase properties within the urban plume from Malmö, and their influence on climate and population health.

ACPD
10, 18661–18730, 2010

ADCHEM includes both vertical and horizontal dispersion perpendicular to an air mass trajectory (2-space dimensions), which is not treated in Lagrangian box-models (0-space dimensions). The Lagrangian approach allows a more detailed representation of the aerosol dynamics, particle and gas phase chemistry and a finer spatial and temporal resolution than available in regional three-dimensional chemical transport models (3D-CTMs). These features make it ideally suited both for studies of urban plumes as well as long distance transported air masses (e.g. studies of regional new particle formation events). The disadvantage with the Lagrangian approach is that the trajectory follows the center of mass of a moving air mass, and does not account for different wind speed or wind directions at different altitudes. Hence, this model approach is not preferable during all meteorological conditions, and if the emissions within a source region (e.g. a city) shows rapid and large temporal variability.

Aerosol models can be divided into equilibrium models and dynamic models. The equilibrium models assume equilibrium between the gas and particle phase while dynamic models treat the mass transport between gas and particle phase. Due to computational limitations the detailed aerosol inorganic chemistry models are primarily equilibrium models, e.g. AIM (Wexler and Clegg, 2002), while aerosol dynamic models usually use a more simplified particle chemistry, e.g. UHMA (Korhonen et al., 2004b), or no particle chemistry, e.g. AEROFOR (Pirjola, 1999) and MONO32 (Pirjola et al., 2003).

Once introducing particle chemistry into the aerosol dynamic model it should preferably be coupled to a detailed gas phase chemistry model. One such early study was performed by Pirjola and Kulmala (1998), which modeled binary H_2SO_4-H_2O nucleation in urban and rural environments, using a box model. Fitzgerald et al. (1998) developed the MARBLES model, which is a one dimensional (1-D) Lagrangian aerosol dynamic model developed to simulate multicomponent (sulfuric acid, sea salt and crustal material) aerosol composition in the marine boundary layer. However, this model did not include a detailed gas phase chemistry model.

ACPD
10, 18661–18730, 2010

Boy et al. (2006) were among the first to include a detailed aerosol dynamic model (UHMA) together with a detailed gas phase chemistry model and a meteorological model in 1-D (vertical). This model named MALTE is primarily designed to model new particle formation in the lower troposphere. ADCHEM developed in this work has many similarities with MALTE concerning the aerosol dynamics, gas phase chemistry and dispersion in the vertical direction. In ADCHEM a second horizontal space dimension was introduced to enable the simulation of horizontal inhomogeneous emissions in urban plumes. However, ADCHEM does not include any meteorological model, and therefore relies on meteorological input data like vertical temperature, relative humidity, wind speed and boundary layer height along the trajectory. ADCHEM also incorporates a detailed radiative transfer model which treats scattering and absorption from gases, particles and clouds (Toon et al., 1989). The gas phase model included in ADCHEM is developed from the kinetic code incorporated in the model developed by Pirjola and Kulmala (1998).

Recently aerosol dynamic models which treat condensation and evaporation of semi-volatile inorganic gases like ammonia (NH_3), nitric acid (HNO_3) and hydrochloric acid (HCl) have been developed (e.g. Zhang and Wexler, 2008). These models can treat the acid and base mass transfer either as separate processes or simplified as a coupled process. The large advantage of coupling the condensation and evaporation of acid and base (e.g. HNO_3 and NH_3) is that the condensation and evaporation becomes pH independent, and allows the model to take longer time steps when solving the condensation/evaporation process. One disadvantage with the coupled condensation/evaporation process is that it is only valid if the aerosol is near acid neutrality (Zaveri et al., 2008 and Zhang and Wexler, 2008).

To be able to take longer time steps (minutes), without causing oscillatory solutions when solving the condensation/evaporation of acid and base as separate processes Jacobson (2005a) developed the prediction of non-equilibrium growth (PNG) scheme. With this method the condensation (dissolution) and evaporation of HNO_3, HCl and H_2SO_4 is solved first, depending on the pH calculated from the previous time step, and

ACPD
10, 18661–18730, 2010

then the NH_3 dissolution is treated as an equilibrium process. With this method the dissolution of NH_3 is linked to the condensation/evaporation of the acids but also depends on the pH in the aerosol liquid phase. Therefore this method is also valid when the aerosol is not near acid neutralized. In ADCHEM, the condensation and evaporation of HNO_3, HCl and NH_3can either be treated as coupled or uncoupled processes and either treating the dissolution of NH_3 as a dynamic or equilibrium process. ADCHEM also considers in-cloud processing of aerosol particles, including sulfate (S(VI)) formation from dissolved SO_2 and H_2O_2. The dissolution of SO_2 and H_2O_2 are treated as equilibrium processes.

The main objective of this work was to develop a model which can be used for detailed simulation of ageing processes within urban plumes, from local scale (1×1 km^2) to regional or global scale. One application of this comprehensive model which is addressed in this work is to study which processes that are most important for accurate representation of aerosol dynamics and particle chemical composition in urban plumes. These results are useful when developing more simplified aerosol dynamics, gas and particle phase chemistry modules or parameterizations for 3D-CTMs or global climate models.

2 Model description

ADCHEM can be divided into three sub-models:

1. an aerosol dynamics and particle chemistry model,
2. a chemical gas phase model,
3. a radiative transfer model.

The aerosol dynamic model in ADCHEM is a sectional model which discretizes the particle number size distribution into finite size bins. The particles are assumed to be internally mixed which means that particles of the same size within the same grid cell

ACPD
10, 18661–18730, 2010

have the same composition. The model includes Brownian coagulation, dry deposition, wet deposition, in-cloud processing, condensation, evaporation, primary particle emissions, homogeneous nucleation and dispersion in the vertical (1-D model) and horizontal direction (2-D model) perpendicular to the air mass trajectory path. The model treats both organic and inorganic particle chemistry with sulfate, nitrate, ammonium, sodium, chloride, non water soluble minerals (metal oxides/hydroxides), soot, Primary Organic Aerosol (POA), Anthropogenic and Biogenic Secondary Organic Aerosol (ASOA and BSOA), and dissolution of sulfur dioxide and hydrogen peroxide into the particles and cloud droplets. In ADCHEM SOA can either be formed by condensation of oxidation products of specific VOCs (e.g. α-pinene, β-pinene, Δ3-carene, D-limonene, isoprene, benzene, toluene and xylene), using the traditional 2-product model (Odum et al., 1996) or using the newly developed volatility basis set (VBS) approach (Donahue et al., 2006), which divides all organic compounds into volatility classes without identifying individual compounds. The aerosol dynamics and particle chemistry model is coupled to the gas phase chemistry model through condensation, evaporation and homogeneous nucleation.

The gas phase chemistry model calculates the gas phase concentrations of 63 different species, using 119 different chemical reactions. Daily isoprene and monoterpene emissions from European forests were simulated separately with the vegetation model LPJ-GUESS (Smith et al., 2001 and Sitch et al., 2003), in which process-based algorithms of terpenoid emissions were included (Arneth et al., 2007; Schurgers et al., 2009a). The emissions from natural vegetation were corrected for anthropogenic land cover following Ramankutty et al. (2008), in a way similar to that in Arneth et al. (2008).

The actinic flux used to calculate the photochemical reaction rates, is derived with the radiative transfer model. This model uses a quadrature two-stream approximation scheme, where the radiative fluxes are approximated with one upward and one downward flux component. The model can be used to calculate the radiative transfer in a vertically inhomogeneous atmosphere with clouds and aerosol particles (Toon et al., 1989).

ACPD
10, 18661–18730, 2010

Figure 1 illustrates the model structure in ADCHEM. The model starts by calculating the turbulent diffusivity in the vertical and horizontal direction using meteorological and land use category input data. After this the model starts integrating over time using operator splitting for each individual process (module). Each individual process (module) displayed in Fig. 1 is described in detail below.

To our knowledge there are no other models available like ADCHEM which combine schemes of detailed aerosol dynamics, gas phase chemistry, inorganic particle phase chemistry, dynamic SOA formation, cloud processing and radiative transfer in 2 space dimensions in a Lagrange model with high spatial and temporal resolution (~1 km, 1 min).

2.1 Atmospheric diffusion

For the simulations performed in this study a model domain of 20 vertical grid cells and 20 horizontal grid cells was used. The vertical and horizontal grid resolution was 100 m and 1000 m, respectively. The 2-D model solves the atmospheric diffusion equation (Eq. 1) in the vertical and horizontal direction perpendicular to the air mass trajectory.

$$\frac{dc}{dt} = \frac{\partial}{\partial z}(K_{zz}\frac{\partial c}{\partial z}) + \frac{\partial}{\partial y}(K_{yy}\frac{\partial c}{\partial y}) \quad (1)$$

Dry deposition and emissions of primary particles in the surface layer are treated separately, and are not included in the boundary conditions for the atmospheric diffusion equation in order to reduce computing time. Instead of solving the 2-D atmospheric diffusion equation for each particle size bin, for 13 different compounds, and each gas phase species (63 compounds), the model solves the atmospheric diffusion equation once for each grid cell. For the 20×20 grid, this means that the diffusion equation has to be solved 400 times in each time step. Equation (1) is solved 400 times by introducing an inert species with initial concentration equal to 1, in one new single grid cell at the time. In all other grid cells the concentration is set to zero. After one time step a new concentration matrix of the inert species is received, which describes the mixing

ACPD
10, 18661–18730, 2010

of the air between the grid cell with initial concentration equal to 1 and the surrounding grid cells. If the time step used is short enough the atmospheric diffusion equation does not have to be solved for the whole grid, but rather for the grid cells closest to the grid cell with an initial concentration equal to 1. This way the simulation time can be decreased drastically.

K_{zz} and K_{yy} in Eq. (1) are the eddy diffusivities (turbulent diffusivities) in the vertical and horizontal direction, respectively. c is the concentration of any arbitrary species. The eddy diffusivities are calculated for stable, neutral and unstable atmospheric conditions using the representations from Businger and Arya (1974); Myrup and Ranzieri (1976) and Tirabassi and Rizza (1997) (Appendix A). The numerical solution of the atmospheric diffusion equation is described in Appendix B. As upper boundary condition the concentration gradient $\partial c/\partial z$ was set to 10^{-3} m^{-1} to account for the generally decreasing gas and particle concentrations above the model domain (2000 m a.g.l.).

2.2 Aerosol dynamics

Each aerosol dynamic process is included as a separate process in the model, using operator splitting. As default the model solves all aerosol dynamic processes with a time interval of 60 s.

2.2.1 Size distribution structures

In ADCHEM the changes in the size distributions upon condensation/evaporation or coagulation are solved with the full-stationary, full-moving or moving-center structures which all have different advantages and disadvantages. All these methods are mass and number conserving, which was tested before the methods were implemented in ADCHEM. For a detailed description of the methods see Sect. 13 in Jacobson, 2005b.

If using the full-stationary structure when calculating how the particle size distribution changes in diameter space the so called splitting procedure has to be used. With

ACPD
10, 18661–18730, 2010

this procedure it is assumed that only a fraction of the particles in one size bin will grow to the next size bin, while the rest of the particles will not grow at all (Korhonen, 2004b). This leads to numerical diffusion which makes the particle size distribution wider and the peak concentration lower (Jacobson, 2005b and Korhonen, 2004b). This is because splitting makes some particles grow more than in the reality, while others will not grow at all. The numerical diffusion can be decreased by increasing the number of size bins (Korhonen, 2004b).

With the full-moving structure the particles are allowed to grow to their exact size and instead of splitting them back onto a fixed diameter grid the diameter grid moves with the particles. While eliminating the numerical diffusion this causes problems if air mixes between adjacent grid cells and if considering new particle formation. Therefore the full-moving structure will not be used in this study.

The moving-center method is a combination of the full-stationary structure and the full-moving structure. The particles are allowed to grow to their exact size as long as they are not crossing the fixed diameter bin limits. If the particles in a size bin cross the lower or upper diameter limit they are all moved to the adjacent diameter bin and their volume is averaged with the particles in the new bin, which then get a new diameter. Since all the particles in one size bin move to a new bin in the same time step the numerical diffusion is minimized when using the moving-center structure. Therefore this method is ideal when the size distribution has to be represented by only a few size bins.

2.2.2 Condensation and evaporation

ADCHEM considers condensation or evaporation of sulfuric acid, ammonia, nitric acid, hydrochloric acid and oxidation products of different organic compounds. Figure 2 illustrates the structure of the condensation/evaporation algorithm used in ADCHEM. The condensation and evaporation is solved by first calculating the single particle molar condensation growth rate of each compound, for each size bin separately (Eq. 2). If considering uncoupled condensation of acids and ammonia the analytic prediction of

ACPD
10, 18661–18730, 2010

condensation (APC) scheme and predictor of non-equilibrium growth (PNG) scheme developed and described in detail by Jacobson (1997, 2005a) are used, while if treating the condensation of acids and ammonia as a coupled process the method first proposed by Wexler and Seinfeld (1990) and later applied by e.g. Zhang and Wexler (2008) is used. The coupled condensation growth rate of NH_3 and HX (mol/s) is given by Eq. (3), where X denotes either Cl or NO_3. The total NH_3 condensation growth rate (I_{NH3}) is then given by the sum of the HCl, HNO_3 and 2 times the S(VI) condensation growth rates ($I_{NH3} = 2I_{S(VI)} + I_{HNO3} + I_{HCl}$). Both methods are mass and number conserving when combined with either the full-stationary, full-moving or moving-center structure. The APC scheme is used for condensation/evaporation of organics, sulfuric acid and for HCl and HNO_3 if they form solid salts with ammonium, while for dissolution of HCl and HNO_3into the particle water phase, the PNG scheme is used instead (Jacobson, 2005a). In this scheme dissolution of ammonia is treated as an equilibrium process solved after the diffusion limited condensation/evaporation of HNO_3, HCl and H_2SO_4. Treating the dissolution of NH_3 as an equilibrium process enables the model to take long time steps (minutes) when solving the condensation/evaporation process (Jacobson, 2005a). This method can easily be modified to treat the ammonia dissolution as a dynamic process. However, this requires that the time step is decreased drastically to prevent oscillatory solutions.

$$I_i = \frac{dc_{p,i}}{dt} = \frac{2D_i D_p}{RT} f_i(Kn_i, \alpha_i)(p_{i\infty} - p_{is})$$
$$f_i(Kn_i, \alpha_i) = \frac{0.75\alpha_i(1+Kn_i)}{Kn_i^2 + Kn_i + 0.283Kn_i\alpha_i + 0.75\alpha_i} \quad (2)$$

$$I_{HX} = \frac{\pi D_p \overline{DC}}{f_{NH_3}} \left(1 - \sqrt{1 - \frac{4f_{NH_3}^2 \left(C_{NH_3,\infty} C_{HX,\infty} - C_{NH_3,s} C_{HX,s}\right)}{\overline{C}^2}}\right)$$
$$\overline{D} = \sqrt{D_{NH_3} D_{HX}} \quad (3)$$
$$\overline{C} = \left(D_{NH_3} C_{NH_3} + D_{HX} C_{NH_3}\right) \Big/ \overline{D}$$

ACPD
10, 18661–18730, 2010

In Eqs. (2) and (3), I_i is the contributions of species i to the mole and diameter growth rates, respectively, f_i is the Fuchs-Sutugin correction factor in the transition region, C_i is the gas phase concentration of species i in moles m^{-3} air, D_p is the particle diameter, t is the time, T is the temperature, R is the ideal gas constant, Kn_i is the non-dimensional Knudsen number, α_i is the mass accommodation coefficient, $p_{i,\infty}$ is the partial pressure and $p_{i,s}$ is the saturation vapor pressure. The mass accommodation coefficients for HNO_3, NH_3, H_2SO_4, HCl, SO_2, H_2O_2 and organic vapors were set to 0.2, 0.1, 1.0, 0.2, 0.11, 0.23 and 1.0, respectively. For the inorganic compounds these numbers are within the range of values tabulated in Sander et al. (2006) over liquid water at temperatures between 260 and 300 K. As a sensitivity test one simulation was also performed with unity mass accommodation coefficients. Usually it is assumed that the saturation vapor pressure of sulfuric acid is zero (Korhonen, 2004a and Pirjola and Kulmala, 1998). The saturation vapor pressure for all condensable organic compounds was set to zero when using species specific organic mass yields according to the two-product model (see Sect. 2.4). The derived 2-product model yields are applied by multiplying them with the concentration of the oxidation products of BTX, monoterpenes and isoprene to give the gas phase concentrations of the condensing products. This way the mass transfer from gas to particle phase is treated as a dynamic process.

If using the VBS approach (Donahue et al., 2006), the VBS accounts for the vapor pressure of each volatility class (see Sect. 2.4), allowing the organic vapors to be transported to and from the particle surfaces, which is not captured with the 2-product model approach. In ADCHEM the VBS is used to determine the molar saturation concentrations at the actual temperature and total organic mass concentration. The sum of the differences between the saturation concentrations and the actual organic vapor concentrations for each volatility class then gives the concentration gradient which drives the mass transfer to or from the particle phase.

Neither with the 2-product model or VBS method the Kelvin effect was considered. This is because there is no well established method on how to treat particle size dependant gas and particle phase partitioning of organic compounds in combination with the

ACPD
10, 18661–18730, 2010

2-product model or VBS method. Neglecting the Kelvin effect has largest in influence of the growth rate of the nucleation mode particles.

The VBS method gives the amount of SOA formed as a function of the exposure to the oxidation agents (e.g. OH) (Jimenez et al., 2009). This way the SOA formation in the model can be treated as a dynamic process that evolves over time, taking into account that the SOA production depends on the initial volatility of the emissions, the oxidation state of the emissions, the oxidation agent concentration, the time of ageing (exposure time) and meteorological conditions (temperature).

In the 2-product model the SOA formation also depends on the time of ageing and concentration of oxidation agents, but only for the initial oxidation step which then determines the final state of the organic compounds (particle or gas phase). Therefore the 2-product model cannot take into account the fact that more volatile compounds generally need longer time of ageing before they are incorporated into the aerosol phase than less volatile compounds.

The saturation vapor concentrations of ammonia, nitric acid and hydrochloride acid and the equilibrium concentration of sulfuric acid and hydrogen peroxide are calculated using a thermodynamic model described in Sect. 2.2.8.

2.2.3 Coagulation

Coagulation has no direct influence on the total particle mass but is important for the total number concentration, the particle number size distribution and the chemical composition distribution, especially for conditions with high number concentrations of nucleation mode particles and a large accumulation mode which the nucleation mode particles can coagulate onto. In cities such conditions can be found in street canyons near the vehicle emissions. Here coagulation is usually the most important aerosol dynamic process (Jacobson and Seinfeld, 2004). The model used in this article treats primary particle emissions occurring on a spatial resolution of $1 \times 1\,km^2$ and not on the street canyon spatial scale (1–100 m). To account for the initial ageing of the primary particle emissions real-world emission size distributions were used, which take

ACPD
10, 18661–18730, 2010

into account the first minutes of ageing from street-canyon to urban background (see Sect. 2.2.5). This decreases the influence of coagulation on the modeled particle number size distribution, but still coagulation needs to be considered for the transformation of the particle number size distribution on longer time scales (hours). The solution of the Brownian coagulation equations is given in Appendix C. Independently if using the full-stationary or moving-center structure splitting needs to be used to fit the particles back onto the diameter grid.

2.2.4 Dry and wet deposition of particles

The dry deposition of particles is treated as a separate process after the atmospheric diffusion equation has been solved. The dry deposition velocities over land are calculated using a resistance model based on the model by Slinn (1982) (modified by Zhang et al. 2001), while over the ocean the model by Slinn and Slinn (1980) is used. The particle transport is governed by three resistances in series, the surface layer resistance (r_a), the quasi-laminar layer resistance (r_b) and the surface resistance or canopy resistance (r_c). The dry deposition velocity for lager particles also depend on the settling velocity (v_s). If particle losses due to impaction, interception and diffusion are considered to take place in the quasi-laminar layer, the surface resistance can be neglected (Seinfeld and Pandis, 2006). The dry deposition velocity representation is given in Appendix D.

The wet deposition rate (s^{-1}) of different particle sizes are calculated according to the parameterization by Laakso et al. (2003), derived from 6 years of measurements at Hyytiälä field station in southern Finland. The only input to the wet deposition parameterization apart from the particle diameter is the rainfall intensity in $mm\,h^{-1}$. Wet deposition removal of particles is considered for all grid cells below the estimated cloud base.

ACPD
10, 18661–18730, 2010

2.2.5 Primary particle emissions

As for the dry deposition the primary particle emissions in the surface layer are treated as a separate process after the atmospheric diffusion equation has been solved. Primary particle emissions included in the model are:

1. Marine aerosol emissions
2. Non-industrial combustion
3. Road traffic emissions
4. Ship emissions

The marine aerosol particle emissions are calculated using the emission parameterization from Mårtensson et al. (2003). The marine particle chemical composition is assumed to be composed of sodium chloride (NaCl) and POA, with NaCl dominating in the coarse mode and organics dominating in the nucleation and Aitken mode, according to the size resolved chemical analysis of marine aerosol particles at Mace Head during the biological active period (spring, summer and autumn) (O'Dowd et al., 2004).

Size resolved anthropogenic primary particle emissions from non industrial combustion and ship traffic are estimated from $PM_{2.5}$ emissions, by applying an assumed effective particle density of 1000 kg m^{-3} and source specific emission size distributions. The primary particle emissions from road traffic were estimated from NO_x emissions, using a NO_x to particle number conversion factor of 3×10^{14} g^{-1} estimated from data in Kristensson et al. (2004). Table S1 in the online supplementary material gives the lognormal size distribution parameters used for the road, ship and non industrial combustion emissions. The road emission size distribution was adopted from Kristensson et al. (2004) and the chemical composition from Pohjola et al. (2007). The ship emission size distribution was measured by Petzold et al. (2008) and the chemical

ACPD
10, 18661–18730, 2010

composition by Moldanová et al. (2009). For the small scale wood burning emissions, the characteristic size distribution was taken from Kristensson (2005) and the chemical composition from Schauer et al. (2001). The non industrial combustion emissions were assumed to originate entirely from small scale wood combustion. The anthropogenic primary particle emissions are mainly dominated by soot and POA. The emitted particle mass fraction not composed of POA or soot was assumed to be composed of water insoluble minerals (metal oxides/hydroxides). For Denmark and Southern Sweden the anthropogenic $PM_{2.5}$ and NO_x emissions along the trajectories are from Danish National Environmental Research Institute (NERI) and Environmental Dept., City of Malmö (Gustafsson, 2001), respectively (see Sect. 2.3.2). For the rest of Europe the emissions were taken from the European Monitoring and Evaluation Program (EMEP) emission database, for year 2006 (Vestreng et al., 2006). The spatial resolution of the emission data was $50\times50\,km^2$ for the EMEP emissions, $17\times17\,km^2$ for the Danish non-road emissions and $1\times1\,km^2$ for all southern Swedish emissions and Danish road emissions.

2.2.6 Aerosol cloud interaction

Clouds are included in ADCHEM if the modeled solar irradiance at the surface is larger than the solar irradiance predicted by HYSPLIT model (Draxler and Rolph, 2003). The altitude of the clouds is determined from the vertical relative humidity profiles along the trajectories, assuming that clouds are present if the RH>98%. If this relative humidity is not reached within the lower 2000 m of the atmosphere (aerosol dynamic model domain), but the difference between the solar irradiance in ADCHEM (without clouds) and the solar irradiance from the HYSPLIT model still imply that clouds need to be present, the clouds are included above the aerosol dynamic model domain without contact with the modeled aerosol particles.

The cloud droplet size distribution was assumed to be lognormally distributed with a mode diameter of 20 µm and a standard deviation of 1.2 for all conditions. The number of cloud droplets is determined by minimizing the difference between the modeled

ACPD
10, 18661–18730, 2010

solar irradiance at the surface, and the solar irradiance from the HYSPLIT model. E.g. if the modeled solar irradiance from ADCHEM is larger than given by the HYSPLIT model, the cloud droplet number concentration is increased in ADCHEM until the solar irradiance at the surface is equal with the value given by the HYSPLIT model.

2.2.7 Homogeneous nucleation

For all simulations homogeneous nucleation was included, using the kinetic nucleation theory (Eq. 4) (McMurry and Friedlander, 1979 and Kulmala et al., 2006). Stable nucleation clusters with a particle diameter of 1.5 nm ($N_{1.5nm}$) were assumed to be formed, using a correlation coefficient (K) of 3.2×10^{-14} s^{-1} cm^3. This value is the median value from measurements at Hohenpeissenberg in Germany (Paasonen et al., 2009).

$$\frac{dN_{1.5nm}}{dt} = K\,[H_2SO_4]^2 \tag{4}$$

2.2.8 Inorganic particle chemistry and particle water content

The aerosol dynamics and particle chemistry model includes a thermodynamic model. The main purpose of the model is to calculate the saturation vapor pressures (concentrations) of hydrochloride acid, nitric acid and ammonia, and equilibrium concentrations of sulfur dioxide and hydrogen peroxide in the particle or cloud droplet water. In the model it is assumed that the inorganic aerosol particle phase is a pure aqueous solution, even if the relative humidity (RH) in the atmosphere is low. However, if the product of the saturation vapor pressure of ammonia and nitric acid and/or ammonia and hydrochloride acid is lower above a solid ammonium nitrate and/or solid ammonium chloride salt surface than above the aqueous solution, the saturation vapor pressures for ammonia, nitric acid and hydrochloride acid above the solid salt surface are used instead of the saturation vapor pressures above the liquid surface. This method has previously been used by e.g. Zhang and Wexler (2008).

ACPD
10, 18661–18730, 2010

From the modeled particle mole concentrations of ammonium, chloride, sodium, nitrate and sulfate an approximated particle salt composition is estimated for each particle size bin according to the explicit scheme in Appendix E.

Molalities of single salts (m_i^0), for NH_4NO_3, HNO_3, $(NH_4)_2SO_4$, NH_4HSO_4, H_2SO_4, $NaHSO_4$, $(Na)_2SO_4$, NaCl and HCl are calculated according to the parameterizations from Table B.10 in Jacobson (2005b). These parameterizations are high order polynomials as functions of the water activity (a_w). The water mass content (W) in the inorganic particle fraction in each particle size bin is derived using the Zdanovskii-Stokes-Robinson (ZSR) model (Stokes and Robinson, 1966).

The inorganic and organic growth factor (Gf_i and Gf_o) are given by Eqs. (5) and (4), respectively. $V_{p,salt}$ is the dry particle volume of water soluble inorganic salts and ρ_{water} is the density of water. Using Eq. (6), the organic growth factor is 1.2 when the water activity is equal to 0.9.

$$Gf_i = \left(\frac{V_{p,salt} + W/\rho_{water}}{W/\rho_{water}} \right)^{1/3} \quad (5)$$

$$Gf_o = \left(1 + 0.081 \frac{a_w}{(1-a_w)} \right)^{1/3} \quad (6)$$

Once the water content has been calculated the molalities of all ions can be determined. The mean binary solute activity coefficients of each salt in the particle water phase are calculated with the parameters in Table B.9 in Jacobson (2005b). From these binary activity coefficients the mean mixed solute activity coefficients are derived using Bromley's method (Bromley, 1973). The next step is to determine the hydrogen ion concentration in the particle water phase from the ion balance (Eq. 7).

$$[H+] + [NH_4^+] + [Na+] = [NO_3-] + 2[SO_4^{-2}] + [HSO_4^-] + [Cl^-] + [OH^-] + [HCO_3^-] + 2[CO_3^{-2}] \quad (7)$$

ACPD
10, 18661–18730, 2010

The concentrations in Eq. (7) can be replaced with known equilibrium coefficients, activity coefficients, the partial pressure of CO_2 (390 ppmv), the N(-III) concentration ($[NH_3(aq)]+[NH_4^+]$), [S(VI)], [N(V)], ($[HNO_3(aq)]+[NO_3^-]$) and [Cl(I)] ($[HCl(aq)]+[Cl^-]$). The final expression then becomes a 7th order polynomial with $[H^+]$ as the only unknown. The $[H^+]$ is given by the maximum real root of this polynomial.

Finally the saturation vapor pressures of ammonia, nitric acid and hydrochloride acid and the equilibrium concentrations of sulfuric acid, and hydrogen peroxide can be determined using the derived hydrogen ion concentration and the mean mixed solute activity coefficients. The saturation vapor pressures (concentrations) are used when solving the condensation/evaporation equation (Eq. 2). The growth rate due to sulfate production, from the reaction between sulfur dioxide and hydrogen peroxide in the particle water phase, is calculated using Eq. (8) (Seinfeld and Pandis, 2006).

$$\frac{d[\mathrm{S(VI)}]}{dt} = \frac{W \cdot k_{\mathrm{S(IV)}} \cdot [H_2O_2] \gamma_{H_2O_2} \left[HSO_3^-\right] \gamma_{HSO_3^-} \left[H^+\right] \gamma_{H^+}}{(1 + K_{\mathrm{S(IV)}}[H^+]\gamma_{H^+})} (\mathrm{moles/s}) \quad (8)$$

Here, $k_{\mathrm{S(IV)}}$ is the irreversible reaction rate coefficient for the reaction between S(IV) and H_2O_2 in the particle water phase and $K_{\mathrm{S(IV)}}$ is the equilibrium coefficient of S(IV) dissolution.

2.3 Gas phase model

The chemical kinetic code included in the gas phase model is solved with MATLABs® ode15 s solver for stiff ordinary differential equations. This solver uses an adaptive time step length according to the specified error tolerance. Most of the reactions are taken from the kinetic code used in the model by Pirjola and Kulmala (1998) (originally from EMEP). Some new reactions, mainly concerning the oxidation of benzene, toluene and xylene are also included in the kinetic code. The reaction rates were updated for those of the reactions where new rates were found in the literature (Sander et al., 2006; Seinfeld and Pandis, 2006 and Atkinson et al., 2004). Pirjola and Kulmala (1998) included

ACPD
10, 18661–18730, 2010

reactions involving dimethylsulfide (DMS) from the ocean in their model. These reactions were however not considered in the chemical kinetic code used in this work. All natural emission of DMS from the oceans was instead assumed to be sulfur dioxide following Simpson et al. (2003).

The photochemical reactions depend on the spectral actinic flux (photons $cm^{-2}\,s^{-1}\,nm^{-1}$). The actinic flux is the flux of photons from all directions into a volume of air (Seinfeld and Pandis, 2006). The actinic flux (F_a) is calculated using the radiative transfer model described in Sect. 2.5. The photolysis rates are directly proportional to the actinic flux incident on a volume of air (Cotte et al., 1997). The wavelength (λ) dependent absorption cross sections (σ) and quantum yields (Q) for the different gases undergoing photochemical reactions were found in Sander et al. (2006). Equation (9) below gives the photochemical reaction rates for species A.

$$j_A = \sum_i \sigma_A(\lambda_i,T)Q(\lambda_i,T)F_a(\lambda_i)\Delta\lambda_i \quad (9)$$

2.3.1 Dry deposition and wet deposition of gases

As for the particles the dry deposition velocity of gases depends on an aerodynamic resistance (r_a) and a quasi-laminar resistance (r_b) in series. For gases the surface resistance (r_c), is also needed. The surface resistance depends on the surface structure as well as the reactivity of the gas (Wesely, 1989 and Seinfeld and Pandis, 2006). The model for dry deposition velocity of gases is described in Appendix F.

The below cloud scavenging of SO_2, HNO_3, NH_3, H_2O_2 and HCHO are described by the parameterization used in Simpson et al. (2003). For all other gases the below cloud scavenging was assumed to be an insignificant loss mechanism.

2.3.2 Gas phase emissions

The gas phase chemistry model takes into account emissions of Biogenic volatile organic compounds (BVOCs) and anthropogenic VOC (AVOC) emissions, CO, NO_x, sul-

ACPD
10, 18661–18730, 2010

fur dioxide and ammonia. The emission data of anthropogenic organic hydrocarbons are not given for each individual species but rather as total Non-Methane Volatile Organic Carbon (NMVOC) emissions. Source specific emissions of non-aromatic hydrocarbons were estimated from the NMVOC emissions, using Table 4.3., in Simpson et al. (2003). The total anthropogenic aromatic hydrocarbon emissions (by Simpson et al. (2003) considered as *O*−xylene emissions) were divided into toluene, xylene and benzene emissions according to the global emissions estimated by Henze et al. (2008). For road traffic emissions 36.7% of the NMVOC are emitted as aromatic hydrocarbons, while for most of the 9 other emission sources specified in Simpson et al. (2003), the aromatic NMVOC fraction is much smaller. According to Calvert et al. (2002) aromatic hydrocarbons contributes to (~20–30 %) of the total VOC concentration in urban environments.

As for the $PM_{2.5}$ emissions the anthropogenic gas phase emissions were adopted from EMEPs emission database for the year 2006 (Vestreng et al., 2006), except for Denmark and Southern Sweden where the emissions are from Danish National Environmental Research Institute (NERI) and Environmental Dept., City of Malmö (Gustafsson, 2001), respectively. The EMEP emissions have a spatial resolution of $50\times50\,km^2$, the Swedish emissions have a resolution of $1\times1\,km^2$ and the Danish emissions have a resolution of $1\times1\,km^2$ for road emissions and $17\times17\,km^2$ for all other emission sectors. All emissions were divided into the EMEP emission sectors S1 to S11 as well as ship emissions and natural sulfur dioxide emissions. The yearly emissions were multiplied with country specific diurnal, weekly and monthly emission variation factors based on EMEP's data. The monthly variations in the natural emissions of sulfur dioxide from DMS oxidation were considered using the monthly emission variations from Tarrasón et al. (1995).

The BVOC species considered are isoprene, α-pinene, β-pinene, Δ3-carene and D-limonene based on LPJ-GUESS' ability to assign species-specific emission capacities (e.g. Schurgers et al., 2009b and Arneth et al., 2008), and the monoterpene speciation in Steinbrecher et al. (2009). These species are oxidized by OH, O_3 and NO_3. The

ACPD
10, 18661–18730, 2010

products from these reactions are generally less volatile than the initial compounds. Some of them are therefore able to condense after one or several oxidation steps. The fraction of the products that will form SOA is given by a yield factor (Y) (Odum et al., 1996) (Sect. 2.4). BVOCs have a relatively short lifetime (minutes to hours) during the daytime in the troposphere (Atkinson and Arey, 2003). Due to the short lifetime of these compounds the concentrations can be considerably higher close to the ground (at the source) than at the top of the boundary layer. Both for the particle and gas phase chemistry it is important to capture the vertical concentration gradient of BVOCs. The emissions of BVOCs from the ground depend strongly on the biomass density and the vegetation species composition, but also on the canopy temperature and for some compounds and vegetation species the photosynthetic active radiation (PAR) (Guenther, 1997).

The emission of BVOCs from different species can either be described as:

1. Volatilization of stored compounds (depend only on temperature when considering short timescales).

2. VOC emissions directly reflecting VOC production (typically varying with temperature and light).

An example of the second case is the light-dependent production of isoprene in the chloroplast. Most monoterpene emissions, particularly those from conifers, are due to volatilization of stored compound (Guenther, 1997), although in recent years light-dependent emissions of non-stored monoterpenes have been found to take place in many broadleaf trees, and may also occur at least from some monoterpene chemical species in conifer (for discussion see Schurgers et al. (2009a) and references therein).

The emissions of stored and synthesized monoterpenes and isoprene were modeled using the vegetation model LPJ-GUESS in combination with isoprene and monoterpene-production linked to their chloroplastic production following Niinemets et al. (1999, 2002). Monoterpene storage and emissions from storage are described in

ACPD
10, 18661–18730, 2010

Schurgers et al. (2009a). Short-term variations of modeled emissions display the typically observed light and temperature dependence (Arneth et al., 2007). The model's shortest time step is one day and diurnal course of emissions were calculated from the daily totals following well-established empirical functions for temperature and light-dependencies by Guenther (1997). LPJ-GUESS was applied with 17 tree species and 3 generic shrub and herb types as functional types (Schurgers et al., 2009b). Each of these was associated with an isoprene and monoterpene production potential for standard environmental conditions, implemented as a fractional contribution of photosynthetic electron-transport rate for BVOC production (Niinemets et al., 1999; Arneth et al., 2007). The simulation of tree-species rather than plant functional types allows realistic values of these production capacities to be assigned (Schurgers et al., 2009b). After a 300-year spin-up, the simulation was run for the period 1981–2006 with monthly averaged climate data for Europe from Haylock et al. (2008). For the periods 28 April to 15 October 2005 and 16 May to 28 October 2006 the monthly data were replaced by daily observations to capture the day-to-day variability in emissions. Daily emissions with a spatial resolution of $15' \times 15'$ ($\sim 25 \times 25\,km^2$) were provided for isoprene and 17 different monoterpene species, the speciation of the monoterpenes was done following Steinbrecher et al. (2009). These emissions from natural vegetation were corrected for the presence of land use with land cover data from Ramankutty et al. (2008).

To be able to use the BVOC emissions from LPJ-GUESS in ADCHEM they had to be converted to high-temporal resolution emissions. This was performed with the empirical functions for temperature and light-dependencies from Guenther (1997), using minute resolution temperature and PAR data along the trajectory, and the daily or daytime leaf surface temperature, PAR and emission fluxes from the LPJ-GUESS simulation as standard conditions.

Since the kinetic code in ADCHEM only includes α-pinene, β-pinene, Δ3-carene and D-limonene, the emissions of all other monoterpenes were distributed among the monoterpenes included in the kinetic code, depending on their emission rates.

ACPD
10, 18661–18730, 2010

2.4 Species specific SOA yields and source specific 2D-VBS

The secondary organic aerosol formation in ADCHEM can either be modeled with the traditional two product model approach (Odum et al., 1996), or the recently proposed VBS approach (Donahue et al., 2006 and Robinson et al., 2007). One advantage with the two product model approach is that it models the SOA formation from specific organic compounds, formed from oxidation products of a few well characterized compounds known to form SOA (e.g. oxidation products of monoterpenes, isoprene, benzene, toluene and xylene). However the SOA formation in the atmosphere is complex and involves thousands of unknown compounds (Donahue et al., 2006).

The VBS scheme lumps all organic species into different bins according to their volatility (given by their saturation concentration (C^*), at 298 K) (Robinson et al., 2007). This method thereby generally loses the information of the chemical reactions in where individual organic compounds are involved in, but is designed to be able to predict realistic SOA formation rates found in the atmosphere using a model with relatively low complexity and only a few model parameters.

Lately, Jimenez et al. (2009) developed a 2D-VBS method which apart from classifying the organic compounds according to their volatility also includes the second dimension, oxygen to carbon ratio (O/C-ratio). This 2D-VBS method is implemented in ADCHEM, with slightly different assumptions which will be described below.

According to the two-product model developed by Odum et al. (1996) the aerosol yield (Y) can be calculated as a function of the aerosol organic mass according to Eq. (10).

$$Y = M_o \left(\frac{\alpha_1 K_{\mathrm{om},1}}{1 + K_{\mathrm{om},1} M_o} + \frac{\alpha_2 K_{\mathrm{om},2}}{1 + K_{\mathrm{om},2} M_o} \right) \quad (10)$$

M_o is the organic particle mass in $\mu g\, m^{-3}$, $K_{\mathrm{om},i}$ is the partitioning coefficient of product i, α_i is the mass based stochiometric yield of product i. Values of α_i and $K_{\mathrm{om},i}$ from Griffin et al. (1999), Svendby et al. (2008), Henze and Seinfeld (2006) and Ng et

ACPD
10, 18661–18730, 2010

al. (2007) are given in Table S2 in the online supplementary material, for all organic oxidation products forming secondary organic aerosol in the model. Benzene, toluene and xylene first react with OH followed by either reaction with NO, forming products with a low and temperature dependent SOA-yield, or with HO_2, which gives products which has a high and temperature independent SOA-yield (at least for M_o >10μg/m^3) (Ng et al., 2007). In this study the SOA yields through the HO_2-pathway were assumed to be constant also below 10 μg/m^3 M_o. At high NO_x/HO_2 ratio, which generally is the case in urban environments, most of the oxidation products will react with NO, while at remote regions the HO_2-pathway will dominate. Therefore, oxidation of benzene, toluene and xylene (BTX) in urban environments generally gives relatively low SOA formation, while moving further away from the source the SOA formation can be considerably higher. Here it is mainly benzene, which is the least reactive of the three compounds, that is left to form SOA (Henze et al., 2008).

Temperature and mass dependent yields for α-pinene, β-pinene, xylene and toluene were taken from Svendby et al. (2008), which modeled the SOA formation using temperature dependent partitioning coefficients according to Eq. (11) from e.g. Sheehan and Bowman (2001). The heats of vaporization (ΔH) of the two product model compounds formed from oxidation of benzene through the NO-pathway were assumed to be the same as for toluene.

$$K_{\mathrm{om}}(T) = K_{\mathrm{om,ref}} \frac{T}{T_{\mathrm{ref}}} \exp\left[\frac{\Delta H}{R}\left(\frac{1}{T} - \frac{1}{T_{\mathrm{ref}}}\right)\right] \quad (11)$$

The 2D-VBS scheme used in ADCHEM classifies the organic compounds into 16 discrete volatility bins, separated by powers of 10 in C^*, ranging from 10^{-4} to 10^{11} μg m^{-3} and 11 discrete O/C-ratio, separated by 0.1, from 0 to 1 (in total 176 (11·16) bins). The mass fraction F_i in the particle phase in each volatility bin i is given by Eq. (12) (Donahue et al., 2006).

$$F_i = (1 + C_i^*/M_o)^{-1} \quad (12)$$

ACPD
10, 18661–18730, 2010

For compounds with C^* equal to 1 µg m^{-3}, Eq. (10) indicates that 50% of these compounds will be found in the particle phase and 50% in the gas phase, if the total particle organic mass content (M_o) is equal to 1 µg m^{-3}.

The temperature dependence of C^* is given by Eq. (11) if K_{om} is replaced with C^*. The heat of vaporization is calculated with a recently proposed expression (Eq. 13) which states that the heat of vaporization can be estimated as a function of the saturation concentration (Epstein et al., 2010). C^*_{300}in Eq. (13) is the saturation concentration at 300 K.

$$\Delta H = -11 \cdot \log_{10} C^*_{300} + 129 \text{kJmol}^{-1} \quad (13)$$

Source specific 2D-VBS emissions from all EMEP source types (S1 to S11 and ship traffic) were estimated from the source specific anthropogenic NMVOC emissions (see Sect. 2.3.2). The non oxidized BVOCs and AVOCs were distributed in the volatility bins of C^* between 10^7 and 10^{11} µg m^{-3} and O/C-ratio equal to 0, with the traditional SOA precursors monoterpenes, isoprene, benzene, toluene and xylene having a C^* of between 10^7 and 10^9µg m^{-3} at 298 K.

Once emitted into the atmosphere the organic compounds can be oxidized by OH, NO_3 and O_3. Jimenez et al. (2009) assumed that all organic compounds after the first oxidation step react with the OH radical with a gas-phase rate constant (k_{OH}) of 3×10^{-11} cm^3 molecules^{-1} s^{-1}, and state that the heterogeneous oxidation rate of organic compounds in the gas phase is at least 10 times slower. In ADCHEM the emitted compounds in each 2D-VBS bin for each source type was divided into fast oxidized (k_{OH} =3×10^{-11} cm^3 molecules^{-1} s^{-1}) or slowly oxidized compounds (k=$3\cdot10^{-12}$ cm^3 molecules^{-1} s^{-1}). Among the fast oxidized compounds are monoterpenes, isoprene, xylene, and all alkenes while among the slowly oxidized compounds are benzene, toluene and all alkanes. The heterogeneous reactions were assumed to be 100 times slower than in the gas phase.

After one or a few oxidation reactions in the atmosphere the oxidation products lose their original signature and become increasingly similar in structure independent of the

ACPD
10, 18661–18730, 2010

original molecular structure (Jimenez et al., 2009). Therefore, for all compounds with O/C-ratio larger than 0, the same k_{OH} of 3×10^{-11} cm^3 molecules^{-1} s^{-1} as proposed by Jimenez et al. (2009) was used in ADCHEM. All compounds except the alkanes and anthropogenic aromatic compounds (BTX) in each 2D-VBS bin were also assumed to be oxidized by O_3 and NO_3 with $k_{O3}=10^{-17}$ cm^3 molecules^{-1} s^{-1}and $k_{NO3}=10^{-14}$ cm^3 molecules^{-1} s^{-1}, which are approximately the reaction rates for alkenes (Atkinson, 1997).

One large uncertainty with the VBS model approach is how to estimate the fraction of the oxidation reactions which cause the organic molecules to fragmentize (form products with lower carbon number and higher O/C-ratio) and which fraction that functionalizes (form new products with the same carbon number and higher O/C-ratio). Jimenez et al. (2009) proposed that the fraction of reactions that cause fragmentation can be given as a function of the O/C-ratio according to Eq. (14), where n in Eq. (14) was assumed to be 6 during low NO_x conditions.

In the 2D-VBS model used in ADCHEM the parameter n was used as a free parameter to fit the modeled aerosol mass yield with the 2D-VBS to the measured aerosol mass yield of benzene, toluene and xylene from Ng et al. (2007) at low and high NO_x conditions. With n equal to 6 the model gave good agreement with the measured toluene and xylene aerosol mass yield at high NO_x conditions, and was therefore used for all oxidation reactions during high NO_x conditions while for the low NO_x conditions the 2D-VBS model gave better agreement with the measured yields if n was assumed to be a function of the O/C-ratio according to Eq. (15). Figure S1 in the supplementary material compares the modeled yields with the 2-product model parameterization of the measured BTX yields from Ng et al. (2007).

For atmospheric relevant particle organic mass concentrations (1–10 µg/m^3) the yield for BTX and monoterpenes with the 2D-VBS is about 2–7% for high NO_x conditions, while 15–25 % for low NO_x conditions, at 300 K. This can be compared with the 2-product model SOA yields of 5–15% for benzene, 2–8% for toluene and 1–4% for xylene at high NO_x conditions and 37 % for benzene, 36 % for toluene and 30% for

ACPD
10, 18661–18730, 2010

xylene at low NO_x conditions.

$$f = \left(\frac{O}{C}\right)^{1/n}, n = 6 \text{ for low } NO_x \text{ conditions} \quad (14)$$

$$n = \frac{O}{C} + \frac{2}{5}\left(\frac{O}{C}\right)^{0.23} + 0.01 \text{ for high } NO_x \text{ conditions} \quad (15)$$

Another key uncertainty in the modeled organic aerosol formation in urban environments is the volatility of the organic emissions traditional considered to be POA (e.g. Shrivastava et al., 2008 and Tsimpidi et al., 2010). Shrivastava et al. (2008) used the 3D-CTM model PMCAMx to model the organic aerosol in the US by either treating these traditional POA emissions as non-volatile (C^*=0) or as semi-volatile (C^* between 10^{-2} and $10^4\,\mu g\,m^{-3}$). Their results illustrate that condensation of oxidized organic compounds formed from compounds which first evaporates after dilution and then are oxidized in the atmosphere has the potential to significantly increase the summertime organic aerosol (OA) in urban environments in US. In this work the traditional POA emissions (e.g. from EMEP) was either treated as non-volatile compounds (C^*=0 $\mu g\,m^{-3}$) or as semi-volatile. These semi-volatile POA (SVPOA) mass emissions were divided into different C^* channels according to the work by Robinson et al. (2007), Shrivastava et al. (2008) and Tsimpidi et al. (2010). Analogous with Robinson et al. (2007), Shrivastava et al. (2008) and Tsimpidi et al. (2010) the intermediate volatile organic carbon (IVOC) emissions (C^* between 10^4 and $10^6\,\mu g\,m^{-3}$), was assumed to be proportional and 1.5 times larger than the POA emissions (see Table S3 in the online supplementary material).

In this work the initial evaporation of particulate organic material because of dilution was not treated by the model with the assumption that this evaporation is a fast process (not significantly mass transfer limited). However, recently performed chamber measurements on wood smoke and diesel car POA emissions indicate that the POA may evaporate slowly before reaching an equilibrium with the gas phase (at least 1 h)

ACPD
10, 18661–18730, 2010

(Grieshop et al., 2009). The spatial and temporal resolution used in ADCHEM enables the treatment of this mass transfer limited evaporation, however more chamber studies at atmospheric relevant conditions are needed before these results can be accurately implemented in ADCHEM.

2.5 Radiative transfer model

The radiative transfer model is mainly used to calculate photolysis rate coefficients for the gas phase chemistry model and to estimate the presence of clouds. The radiative transfer model uses the quadrature two-stream approximation scheme, where the radiative fluxes are approximated with an upward and downward flux component. The phase function and the angular integral of the intensity field are approximated using the asymmetry parameter (g) and single scattering albedo (w_0). The model can be used to calculate the radiative transfer in a vertically inhomogeneous atmosphere with clouds and aerosols (Toon et al., 1989). The asymmetry parameter and single scattering albedo for aerosol particles and cloud drops is calculated using a Mie-theory model. The radiative transfer model is described more in detail in Appendix G.

3 Methods for urban plume studies

In this section the methods used when modeling the properties of the aerosol particles inside the urban plume from Malmö are described briefly. For a more detailed description of these methods, see Roldin et al. (2010). The model is applied here for one case study, to test the model performance and to illustrate the spatial and temporal variability of the aerosol properties within the urban plume from Malmö.

3.1 Measurements

Particle and/or gas concentrations measured at three different stations in Sweden were either used to validate the model performance or as input to the model. The first station

ACPD
10, 18661–18730, 2010

is an urban background station positioned in Malmö (55° 36′ N, 13° 00′ E, 30 m a.s.l.), the second station is the EMEP background station at Vavihill (56° 01′ N, 13° 09′ E, 172 m a.s.l.), about 50 km north from Malmö, and the third station is the EMEP background station at Aspvreten (17° 23′ N, 58° 48′ E, 20 m a.s.l.), about 450 km north-east from Malmö. Descriptions of the measurement stations at Vavihill and Aspvreten can be found in Kristensson et al. (2008) and Tunved et al. (2004), respectively.

The selected case study in this article is from 21 June 2006. Figure 3 displays the selected air mass trajectory for this case. The trajectory was derived with the HYSPLIT model (Draxler and Rolph, 2003). It arrives at 100 m a.g.l. in Malmö, at 06:00 a.m. and passes over Vavihill background station around 09:00 a.m.. The trajectory started over England, 48 h upwind Malmö and end 24 h downwind Malmö close to Stockholm. Locations A, B and C in Fig. 3 are Malmö, Vavihill and Aspvreten respectively. The trajectory does not pass over Aspvreten, but about 50 km east from the station. Therefore it is unlikely that the urban emissions in Malmö influenced Aspvreten this time of the day. Still the measured ozone level at Aspvreten was used to check if the magnitude of the modeled ozone concentration was reasonable, with the assumption that the background ozone level is relatively uniform over large regional areas.

The particle number size distributions in Malmö and Vavihill were measured with a Scanning Mobility Particle Sizer (SMPS) and a Twin Differential Mobility Particle Sizer (TDMPS). The SMPS system in Malmö measured the urban background particle number size distribution from 10 to 660 nm at a roof top station about 20 m a.g.l, at the town hall in the north-west part downtown Malmö. During southerly air masses this station picks up most of the particle emissions from Malmö. A description of the SMPS system in Malmö can be found in Roldin et al. (2010).

The TDMPS system at Vavihill field station measures the rural background particle number size distribution from 3 to 900 nm every 10 minutes. A detailed description of the TDMPS at Vavihill can be found in Kristensson et al. (2008).

Measured concentrations of NO, NO_2, O_3 and SO_2 at the urban background station in Malmö and O_3 at Vavihill were compared with the modeled gas phase concentrations

ACPD
10, 18661–18730, 2010

along the trajectory (for more information about the gas phase measurements see Roldin et al., 2010).

Apart from measured particle and gas concentrations, wind direction measurements from a meteorological mast in Malmö were used to verify that the urban plume from Malmö was directed toward Vavihill. The wind direction was measured at 24 m a.g.l.

3.2 Model input

Vertical temperature, wind speed and relative humidity profiles, rainfall intensity, mixing height and emissions of isoprene, monoterpenes, anthropogenic NMVOCs, NO_x, SO_2, CO, NH_3 and $PM_{2.5}$ were included along the trajectories (for more information see Roldin et al. (2010) and references therein).

The initial particle number size distributions in ADCHEM were estimated from the measured background particle number size distribution at Vavihill, according to the method described in Roldin et al. (2010). Initially (48 h upwind Malmö) the $PM_{2.5}$ mass fractions of each compound were estimated to be: 0.36 organics, 0.08 soot, 0.25 sulfate, 0.17 nitrate and 0.14 ammonium below 1000 m a.g.l. and then changing linearly to the top of the model domain (2000 m a.g.l.), to 0.22 organics, 0.05 soot, 0.30 sulfate, 0.25 nitrate and 0.18 ammonium. These values are in reasonable agreement with the measured chemical composition at several European sites in England and Germany (Jimenez et al., 2009). The sodium and chloride concentrations were initially set to zero. Because the model is only initiated 48 hours upwind Malmö, these initial particles properties may influence the particle composition within the urban plume from Malmö, especially for the particles larger than ~1 µm, which have a long lifetime and relatively small sources.

3.3 Spin-up time before Malmö

The total run time of the simulations was 3 days, starting 2 days before the air mass trajectory reached Malmö and continuing 1 day downwind Malmö. The first two days

ACPD
10, 18661–18730, 2010

of the simulation were used to initialize the particle and gas phase chemistry. During these days the particle number size distribution was kept fixed, while everything else was allowed to change. Once the trajectories reach the southern border of Malmö the estimated local road emission contributions from the size distribution measurements in Malmö were included according to the method described in Roldin et al. (2010). With this method the modeled particle number size distribution at the measurement station in Malmö become comparable with the measured distribution at that time. After the urban background station in Malmö, the particle number size distributions were allowed to change due to the aerosol dynamic processes, and vertical and horizontal mixing.

4 Results and discussion

Results from 18 separate model simulations will be compared and discussed. The simulations were designed to study the influence of (1) different number of size bins, (2) size structure methods, (3) aerosol dynamic processes, (4) the effect of coupled or uncoupled condensation, (5) the effect of application of the VBS or traditional 2-product model for secondary aerosol formation, (6) treating POA as semi-volatile (SVPOA) with C^* between 10^{-2} and 10^4 µg/m^3 or non-volatile, (7) including intermediate volatile organic carbon (IVOC) emissions with C^* between 10^4-10^6 µg/m^3 and (8) horizontal and vertical mixing. The model runs are listed below. If not otherwise specified the full-stationary structure with 200 size bins was used, condensation/evaporation was solved as an uncoupled process, both vertical and horizontal mixing was considered, the 2D-VBS method was used for the partitioning of organic compounds between gas and particle phase, POA was assumed to be non-volatile and IVOC emissions were not considered.

1. All processes included (base case)
2. Full-stationary structure with 50 size bins

ACPD
10, 18661–18730, 2010

3. Full-stationary structure with 25 size bins
4. Moving-center structure with 25 size bins
5. Moving-center structure with 10 size bins
6. Combination of full-stationary and moving-center with 25 size bins
7. Coupled condensation
8. 2-product model used for SOA production
9. No aerosol dynamic processes
10. No dry deposition
11. No coagulation
12. No condensation growth
13. No wet deposition
14. Doubled mixing height.
15. Doubled horizontal turbulent diffusivity
16. 1-D model (without horizontal mixing)
17. With SVPOA and IVOC emissions
18. Unity mass accommodation coefficients

In Fig. 4a–b the modeled particle number size distributions at Vavihill (3 h downwind Malmö) and 24 h downwind Malmö, for different number of size bins and size structure methods, are compared. Given is also the measured particle number size distribution at Vavihill, at the time of arrival of the air mass trajectory. The given particle number

ACPD
10, 18661–18730, 2010

size distributions are from the center of the urban plume in the surface layer. At Vavihill (Fig. 4a) all simulations are in good agreement with each other and the measured particle number size distribution. This illustrates that for short time scales (a few hours) the model results are fairly insensitive to the number of size bins and size structure which is used, especially if the condensation or evaporation rates are small. 24 h downwind Malmö (Fig. 4b) the difference between the simulations becomes more evident. This is especially the case for the moving-center method and the full-stationary method when using 25 size bins. For the full-stationary method with 25 size bins, the numerical diffusion significantly broadens the size distribution (see Sect. 2.2.1). With the moving-center method errors can appear when the particles from the lower size bins are averaged with the particles in higher size bins, which causes some bins to get too low concentrations (zero concentration) while bordering size bins get too high concentrations. In Fig. 4b this can be seen around 600 nm in diameter. For the moving-center method this problem is solved by decreasing the number of size bins, while for the full-stationary method the accuracy increases with the number of size bins. Figure 4a–b also shows the result from one simulation with 25 size bins, where the moving-center method was used except once every 360th time step (6 h) when the full-stationary method was used. This combination of the two methods gives much smaller numerical diffusion than the full-stationary method and still eliminates the problems seen with the moving-center method.

Figure 5a–b compares the modeled particle number size distributions with or without different aerosol dynamic processes at Vavihill and 24 h downwind Malmö. The result without wet deposition is only given at 24 h downwind Malmö since no rainfall affected the size distribution between Malmö and Vavihill. About 2 h after Vavihill a light rainfall (~0.5 mm/h) started and continued for a few hours, which affect the size distribution 24 h downwind Malmö.

The aerosol dynamic processes with largest influence on the particle number size distribution both at Vavihill and 24 h downwind Malmö was dry deposition. This is mainly because of the relatively few nucleation mode particles. Condensation and

ACPD
10, 18661–18730, 2010

evaporation have little influence on the results at Vavihill but have larger influence on the size distribution 24 h downwind Malmö. Using unity mass accommodation coefficients for all condensable compounds instead of the values given in Sect. 2.2.2 had negligible impact on the modeled particle number size distribution and chemical composition (not shown). The primary particle emissions between Malmö and Vavihill have a marginal impact on the size distribution below 30 nm which can be seen when comparing the initial particle number size distribution and the results without aerosol dynamic processes.

When not considering aerosol dynamic processes the size distribution was almost preserved between Malmö and Vavihill. This illustrates that vertical and horizontal mixing had little influence on results in the center of the urban plume, for short time scales. For the vertical mixing, this is partly due to the low and constant boundary layer height at 300 m between Malmö and Vavihill. A rising boundary layer effectively dilutes the boundary layer, which mainly explains why the number concentration is significantly lower 24 h downwind Malmö than in the city, even without any aerosol dynamic processes. Figures 5c–d illustrate the modeled particle number size distributions at Vavihill and 24 h downwind Malmö with doubled mixing height (MH), no horizontal mixing (1-D model) and doubled horizontal eddy diffusivity ($2\times K_y$). These simulations confirm that for at least low or moderate turbulence (stable or neutral conditions) both vertical and horizontal mixing has much smaller impact on the model results than the aerosol dynamic processes. When doubling the mixing height the particle number concentration became slightly higher which mainly is due to the decreasing influence of dry deposition. It is important to mention that the initial particle number size distribution in Malmö within the whole boundary layer was assumed to be the same for both mixing heights.

All the measured gases (NO, NO_2, O_3 and SO_2) were well captured by the model in Malmö, when considering the anthropogenic gas phase emissions in the city (Fig. 6). Unfortunately O_3 measurements were the only gas phase measurements with high time resolution, available at Vavihill and Aspvreten. The modeled O_3 concentration

ACPD
10, 18661–18730, 2010

agrees very well with the measured concentrations at Malmö and Aspvreten, if considering that Aspvreten is not influenced by the urban plume from Malmö. At Vavihill the model seems to overestimate the O_3 concentration with about 20%. The reason for this is not known, but possibly the recovery after the O_3 depletion by NO in Malmö was faster in the model than in the real atmosphere.

The modeled $PM_{2.5}$ of ammonium, nitrate, sulfate, organics and soot, from 6 h before Malmö until 24 h downwind Malmö are given in Fig. 7a. At Malmö there is a significant increase in the soot and organic mass due to the primary particle emissions in the city. The modeled primary particle mass increase over Malmö was constrained by the measurements at the urban background station in Malmö (see Sect. 3.3). Nitrate shows a large temporal variability which correlates with the temperature and relative humidity fluctuations. When considering coupled condensation, the particle nitrate content was smaller while the ammonium content was about the same as for the uncoupled condensation simulations. This is because the particles were not fully neutralized (between 28 and 18% of the sulfate was in the form of bisulfate (HSO_4^-) and the rest SO_4^{-2} in the $PM_{2.5}$ particle water phase), with least neutralized aerosol over the ocean 1–2 h before Malmö).

The organic $PM_{2.5}$ is larger in the 2-product model than the 2D-VBS base case simulation, with a maximum difference of 13% about 20 h downwind Malmö. In this study the ASOA formation with the 2D-VBS model was fitted to the 2-product model yields of BTX from Ng et al. (2007) at high and low NO_x conditions. However, for the modeled total organic particle content (2–4 $\mu g/m^3$) the BTX yields with the VBS was still 40–50% lower than the 2-product model at low NO_x conditions (see Sect. 2.4). Since BTX was the most important volatile ($C^*>10^6\,\mu g/m^3$) ASOA precursors both in the 2-product model and the 2D-VBS this can explain the different results. Given are also the results from the simulation when considering SVPOA and IVOC emissions from anthropogenic sources (see Sect. 2.4). This simulation gives slightly less organic particle mass upwind Malmö than if treating the POA as non-volatile and without IVOC emissions (base case). However, a few hours downwind Malmö a significant fraction of

ACPD
10, 18661–18730, 2010

the SVPOA and IVOC emissions found in the gas phase in Malmö have been oxidized and the OA mass concentration becomes up to 7% higher than for the base case.

The soot particle mass emitted in Malmö is primarily lost by dry deposition between Malmö (06:00 a.m.) and 10:00 a.m. After this the boundary layer starts to rise steeply, which effectively dilutes the boundary layer (Fig. 9e).

Figure S2 in the online supplementary material compares the modeled molar oxygen to carbon ratio (O/C-ratio), in the center of the urban plume, in the surface layer, for the base case simulation and when considering SVPOA and IVOC emissions. For both simulations the O/C-ratios decreases from about 0.4 to 0.3 due to the POA emissions in Malmö, with slightly lower O/C-ratio for the base case. After 10:00 a.m. the O/C-ratios increases quickly back to about 0.38, mainly due to the rising boundary layer.

Figure 7b–c illustrates the modeled mass size distributions of the major particle compounds. Noticeable is that the nitrate content is shifted toward larger particle sizes when using uncoupled condensation while the organic mass is mainly found on smaller particles. This is especially pronounced 24 h downwind Malmö. Similar separation of particulate nitrate and organics on different particle sizes are commonly observed with aerosol mass spectrometer (AMS) at Vavihill (Roldin et al., 2010).

Figure 8 gives the size resolved mass fractions of ammonium, nitrate, sulfate, sodium, soot and organics and the pH, in each size bin, from the reference simulation (see Sect. 4). Ammonium and nitrate are well correlated above 100 nm in diameter and cycle between the accumulation mode and the gas phase, driven by the relative humidity and temperature fluctuations. Sulfate is mainly found in the Aitken and accumulation mode while the organics dominate in the nucleation and Aitken mode comprising between 50 and 90% of the total mass below 50 nm in diameter. The pH of the aerosol showed only small temporal variations but varied with the size of the particles, from 0.5 in the nucleation mode to 2.5 in the coarse mode. These pH-values can be compared with the pH of a fully neutralized particle of 5.6 (at 380 ppmv CO_2). The main reason why pH increases with the particle size is that condensation growth rate of sulfuric acid is independent of the pH and the relative molar condensation growth rate

ACPD
10, 18661–18730, 2010

is approximately proportional to the particle diameter and not to the particle volume. Since the diameter to volume ratio increases with decreasing particle size, the sulfate concentration in the particle water phase decreases with increasing particle diameters. The lower hydrogen ion concentration in the larger particles explains why the nitrate is shifter toward larger particles when using uncoupled condensation but not when using coupled condensation (no pH dependence).

Figure 9 gives the modeled vertical $PM_{2.5}$ profiles of different chemical compounds, in the center of the model domain, 6 h before Malmö until 24 h downwind Malmö. The mixing height is also illustrated. As a complement to Fig. 9, Fig. S3 gives the gas phase concentrations of ammonia, nitric acid, sulfuric acid and NO_x in the vertical direction. The $PM_{2.5}$ nitrate and ammonium have a maximum 5 to 6 h downwind Malmö in the whole boundary layer, explained by the high relative humidity at that time (~90%). In contrast, the gas phase ammonia and nitric acid show a different pattern with maximum concentrations before Malmö, when the RH is lower. The $PM_{2.5}$ sulfate content shows less vertical variability than nitrate and ammonium but is larger above the boundary layer over Malmö than in the boundary layer. The organic part of $PM_{2.5}$ is highest near the ground and up to about 1000 m which is approximately the maximum altitude of the boundary layer upwind Malmö. The soot mass increases quickly over Malmö within the boundary layer but are effectively diluted when the boundary layer rises steeply around 10 am. As expected the NO_x concentration (Fig. S3d) is well correlated with the soot particle mass since both compounds mainly originates from the vehicle emissions in Malmö. Because of the high NO_x concentration in Malmö the SOA formation within the urban plume are clearly dominated by the high NO_x pathway during the day. This is even the case 24 h downwind Malmö.

5 Summary and conclusions

In this work a trajectory model for Aerosol Dynamics, gas phase CHEMistry and radiative transfer calculations (ADCHEM) was developed and evaluated. The model consid-

ACPD
10, 18661–18730, 2010

ers both vertical and horizontal dispersion perpendicular to an air mass trajectory. The Lagrangian approach makes the model computationally faster than available regional 3D-CTMs. This enables a more detailed representation of the aerosol dynamics, gas and particle phase chemistry and a finer spatial resolution. These features make it ideally suited for modeling of ageing processes relevant for climate and health, from local to regional or global scales. Possible ADCHEM applications are:

- Studies of condensation and evaporation of semi-volatile gas phase species (e.g. HNO_3, NH_3, HCl and oxidation products of VOCs).
- Modeling the urban influence on the oxidizing capacity of the atmosphere (e.g. ozone, OH, HO_2, NO_3, NO concentrations affecting the ASOA and BSOA formation).
- Transformation of real-world size-resolved primary particle emissions to a grid scale treated by regional and global 3D-CTMs, accounting for sub-grid scale processes.
- Studies of new particle formation and growth within urban plumes or large scale regional nucleation events.
- Estimating the urban influence on cloud condensation nuclei (CCN) properties (indirect effect).
- Studies of the urban emissions influence on the aerosol optical properties and radiative balance (direct effect).
- Population exposure and respiratory dose studies.

When using more than 50 size bins between 1.5 and 2500 nm the full-stationary method gave relatively little numerical diffusion, while when using only 10 size bins the moving-center method which almost eliminates numerical diffusion was a better choice. When using around 25 size bins neither of these two methods were ideal, but a

ACPD
10, 18661–18730, 2010

combination of the two methods gave good representation of the particle number size distribution.

The 2D-VBS method and the 2-product model gave similar organic mass content in the particle phase when POA was treated as non-volatile. This is not surprising since the major SOA precursors considered are the same in both the 2-product model and 2D-VBS approach and the 2D-VBS yields of BTX were fitted to the new 2-product model SOA yields from Ng et al. (2007) (see Sect. 2.4). Lane et al. (2008) compared the modeled organic aerosol from the PMCAMx 3D-CTM using the 2-product model or VBS approach and concluded that the model framework (e.g. 2-product model or VBS) are less important than the parameters used in the model (e.g. saturation concentrations and yields).

One large advantage with the VBS method is that the traditional POA emissions can be treated as semi-volatile, with potentially large influence on the modeled organic mass content. However, for the case studied in this article the evaporation and condensation of oxidized SVPOA and IVOCs had relatively small influence on the organic aerosol mass, composition and size distribution up to 24 h downwind Malmö.

When using uncoupled condensation, significantly more particle phase nitrate was formed than if assuming coupled condensation. The particle nitrate is also shifted towards larger particle sizes for uncoupled condensation compared to coupled condensation. These differences occurred since the aerosol particles were not fully neutralized and the pH increases with the particle size. This illustrates that coupled condensation should not be used if the aerosol particles are not fully neutralized.

For the considered case study the air mass trajectory spent much time over the ocean before arriving in Malmö (see Fig. 3). Here there are no or very small emissions of ammonia but relatively large emissions of SO_2 from ship traffic. This can explain why the aerosol particles were not fully neutralized. If the air mass instead would have been traveling over the large agricultural areas in Europe the aerosol would likely have been more neutralized and the agreement between the uncoupled and coupled condensation simulations would have been better.

ACPD
10, 18661–18730, 2010

Without rainfall, in-cloud processing and rising boundary layer height the particle number size distribution within the center of the urban plume from Malmö can likely be modeled accurately with a box-model (0-D) by only considering dry deposition, coagulation and condensation. If the mixing height on the other hand rises during the day it is also important to consider vertical mixing. Horizontal mixing seems to have small influence on the particle number size distribution in the center of the urban plume up to 50 km downwind Malmö, at least during stable or neutral atmospheric conditions.

For more information about the Malmö emissions influence on climate and health relevant particle properties within the urban plume, the reader is referred to Roldin et al. (2010), where ADCHEM is applied to 26 trajectories for the period April 2005 to October 2006.

Appendix A

Atmospheric diffusion

The kinematic heat flux (F_H) is used in the model when calculating the eddy diffusivity coefficients and the dry deposition velocities. The kinematic heat flux in the surface layer can be approximated with Eq. (A1) (Stull Appendix H, 2000).

$$F_H = -K_H \cdot \frac{\Delta\theta}{\Delta z}, K_H = \kappa^2 \cdot z^2 \cdot \left| \frac{\Delta v}{\Delta z} \right| \quad \text{(A1)}$$

v is the horizontal wind speed, κ is the von Kármán constant, K_H is the heat eddy viscosity, z is the altitude and θ is the potential temperature.

The eddy diffusivity in the vertical direction in the boundary layer is calculated using Eqs. (A2), (A3) and (A4) for stable, near neutral and unstable conditions, respectively. Equation (A2) is adopted from Businger and Arya, 1974, Eq. (A3) from Myrup and Ranzieri, 1976 and Eq. (A4) from Tirabassi and Rizza, 1997. Above the boundary

ACPD
10, 18661–18730, 2010

layer the eddy diffusivity is approximated using Eq. (A2).

$$K_{zz} = \frac{\kappa u_* z}{0.74 + 4.7(z/L)} \exp\left(\frac{-8fz}{u_*}\right) \frac{h}{L} > 10 \quad \text{(A2)}$$

$$K_{zz} = \begin{cases} \kappa u_* z \frac{z}{h} < 0.1 \\ \qquad\qquad -10 \le \frac{h}{L} \le 10 \\ \kappa u_* z (1.1 - \frac{z}{h}) \qquad 0.1 \le \frac{z}{h} \le 1 \end{cases} \quad \text{(A3)}$$

$$K_{zz} = \kappa w_* z \left(1 - \frac{z}{h}\right) \frac{h}{L} < -10 \quad \text{(A4)}$$

h is the mixing height, u_* is the friction velocity, f is the Coriolis parameter, L is the Monin-Obukhov length and w_* is the convective scaling velocity.

The horizontal eddy diffusivity is estimated using Eq. (A5), if the flux Richardson number is negative (unstable atmosphere) (Seinfeld and Pandis, 2006). If the atmosphere is stable the horizontal diffusivity is set as two times the largest vertical eddy diffusivity (Tirabassi and Rizza, 1997).

$$K_{yy} = 0.1 w_* h \quad \text{(A5)}$$

ACPD
10, 18661–18730, 2010

Appendix B

Numerical solution to the atmospheric diffusion equation

The atmospheric diffusion equation (Eq. 1) is discretized using the second order five-point formula (Eq. B1).

$$\begin{aligned}&\text{For} \quad k=1,\ldots.N, \quad n=1,\ldots.N\\&\frac{\Delta c}{\Delta t}_{k,n} = \frac{1}{\Delta z^2}(K_{zz,k-\frac{1}{2}}c_{k-1,n} + K_{zz,k+\frac{1}{2},n}c_{k+1,n})\\&+\frac{1}{\Delta y^2}(K_{yy,n-\frac{1}{2}}c_{k,n-1} + K_{yy,n+\frac{1}{2}}c_{k,n+1})\\&-\frac{1}{\Delta z^2}(K_{zz,k-\frac{1}{2}} + K_{zz,k+\frac{1}{2}})c_{k,n} - \frac{1}{\Delta y^2}(K_{yy,n-\frac{1}{2}} + K_{yy,n+\frac{1}{2}}) + h_{k,n}\end{aligned} \tag{B1}$$

N is the number of grid cells in the vertical and horizontal direction. $h_{k,n}$ is the rest terms containing the boundary values. If dry deposition and emissions are included directly in the atmospheric diffusion equation these terms will enter here.

The horizontal boundary conditions are the background particle and gas concentrations. If the ground-level emission rate (E) and dry deposition are included in the boundary conditions at the ground they are described by Eq. (B2). The boundary conditions at the top of the vertical model domain are given by Eq. (B3).

$$v_d c - K_{zz}\frac{\partial c}{\partial z} = E \tag{B2}$$

$$\frac{\partial c}{\partial z} = 10^{-3}\,\mathrm{m}^{-1} \tag{B3}$$

v_d and E is the dry deposition velocity and emission of particles or gases.

Equation (B1) can be written in matrix form with one matrix for each space dimension ($\mathbf{T}_z$ and $\mathbf{T}_y$) (Eq. B4).

$$\frac{\Delta c}{\Delta t} = (\frac{1}{\Delta z^2}\mathbf{T}_z + \frac{1}{\Delta y^2}\mathbf{T}_y)\boldsymbol{c} + \boldsymbol{h}_{z,y} \tag{B4}$$

ACPD
10, 18661–18730, 2010

For each time step that the model takes, Eq. (B4) is solved using the second order implicit trapezoidal rule (Crank-Nicolson method). The procedure is described by Iserles, 2004. Equation (B5) is the final expression used to solve the atmospheric diffusion equation in 2-space dimensions.

$$c^{j+1} = \left[1 - \frac{1}{2}\frac{\Delta t}{\Delta z^2}\mathbf{T}_z\right]^{-1}\left[1 + \frac{1}{2}\frac{\Delta t}{\Delta z^2}\mathbf{T}_z\right]\left[1 - \frac{1}{2}\frac{\Delta t}{\Delta y^2}\mathbf{T}_y\right]^{-1} \cdot \left[1 + \frac{1}{2}\frac{\Delta t}{\Delta y^2}\mathbf{T}_y\right]\cdot(c^j + \frac{1}{2}\Delta t \cdot h^j_{z,y}) + \frac{1}{2}\Delta t \cdot h^{j+1}_{z,y} \quad \text{(B5)}$$

Appendix C

Brownian coagulation

The coagulation coefficient between two particles of same or different diameters is given by Eq. (C1). β is the Fuchs correction factor, given by Eq. (C2) (Seinfeld and Pandis, 2006).

$$K_{ij} = 2\pi\beta_{ij}(D_{pi}D_i + D_{pi}D_j + D_{pj}D_i + D_{pj}D_j) \quad \text{(C1)}$$

$$\beta_{ij} = \left[\frac{D_{pi}+D_{pj}}{D_{p1}+D_{pi}+2(\delta_i^2+\delta_j^2)^{1/2}} + \frac{8\alpha(D_i+D_j)}{(\bar{c}_i^2+\bar{c}_j^2)^{1/2}(D_{pi}+D_{pj})}\right]^{-1}$$
$$\bar{c}_i = \left(\frac{8kT}{\pi m_i}\right)^{1/2}, \quad \delta_i = \frac{1}{3D_{pi}l_i}\left[(D_{pi}+l_i)^3 - (D_{pi}^2 + l_i^2)^{3/2}\right] - D_{pi}, \quad l_i = \frac{8D_i}{\pi\bar{c}_i} \quad \text{(C2)}$$

α is the collision efficiency which can be assumed to be 1 for all particle sizes (Clement et al., 1996), m_i is the singe particle mass in size bin i, $\bar{c}_i$ is the mean particle velocity and l_i is the mean free path.

Equation (C1) is used to calculate a matrix containing all possible coagulation rates between two particles with different or equal diameters in the finite diameter size bins considered.

ACPD
10, 18661–18730, 2010

The splitting parameters used to divide the formed single particle volumes into the fixed size bins, are calculated with Eq. (C3).

$$y_{1,i,j} = \frac{(V_{p,i+1} - V_{p,\mathrm{coag},i,j})}{(V_{pi+1} - V_{pi})}, \quad V_{p,\mathrm{coag},i,j} = V_{p,i} + V_{p,j}$$
$$y_{2,i,j} = 1 - y_{1,i,j} \tag{C3}$$

$y_{1,i}$ is the fraction of the single particle volume of the formed particle ($V_{p,\mathrm{coag},i,j}$) which will fall into the smaller size bin i and $y_{2,i}$ is the fraction of particle volume which will fall into the larger size bin $i+1$.

The coagulation sink and source are described by Eqs. (C4) and (C5). Combining the coagulation sources and sinks gives the final equations used to calculate new particle size distributions, in each grid cell (Eq. C6).

$$\mathrm{Coag}_{\mathrm{sink},i,j} = K_{ij} c_i \cdot c_j \tag{C4}$$

$$\mathrm{Coag}_{\mathrm{source},i,j} = a_{i,j} K_{ij} c_i \cdot c_j, \quad \text{if} \quad i = j, \quad a_{i,j} = 0.5, \quad \text{else} \quad a_{i,j} = 1 \tag{C5}$$

$$c_i = c_i + \sum_{j}^{N} (y_{1,i,j} \cdot \mathrm{Coag}_{\mathrm{source},i,j} + y_{2,i-1,j} \cdot \mathrm{Coag}_{\mathrm{source},i-1,j} - \mathrm{Coag}_{\mathrm{sin}k,i,j}) \cdot \Delta t \tag{C6}$$

The volume change of different species (k) in the aerosol particle phase due to coagulation between particles in size bin i and j is derived with Eq. (C7).

$$\frac{dV_{i,j,k}}{dt} = y_{1\,i,j} \cdot \mathrm{Coag}_{\mathrm{source},i,j} \cdot x_{\mathrm{coag}\,i,k} \cdot V_{p,\mathrm{coag},i}$$
$$+ y_{2\,i-1,j} \cdot \mathrm{Coag}_{\mathrm{source},i-1,j} \cdot x_{\mathrm{coag}\,i-1,k} \cdot V_{p,\mathrm{coag},i-1} - \mathrm{Coag}_{\mathrm{sink},i,j} \cdot V_{p,i} \cdot x_{i,k} \tag{C7}$$

$x_{i,k}$ is the volume fraction of species k in size bin i and $x_{\mathrm{coag},i,k}$ is the volume fraction of species k in the formed particle.

ACPD
10, 18661–18730, 2010

Eq. (C8) gives the volume of species k in each size bin.

$$V_{i,k} = V_i \cdot x_{i,k} + \sum_j^N \frac{dV_{i,j,k}}{dt} \cdot \Delta t \quad \text{(C8)}$$

Appendix D

Dry deposition velocities of particles

Equation (D1) gives the dry deposition loss rate (v_d) of particles. r_a is the surface layer resistance, r_b the quasi-laminar layer resistance and v_s is the settling velocity.

$$v_d = \frac{1}{r_a + r_b + r_a r_b v_s} + v_s \quad \text{(D1)}$$

The settling velocity is given by Eq. (D2).

$$v_s = \frac{\rho_p D_p^2 g C_c}{18\mu} \quad \text{(D2)}$$

ρ_p is the particle density, μ is the dynamic viscosity, C_c is the Cunningham slip correction factor and g is the acceleration of gravity

The surface layer resistance can be expressed by Eqs. (D3) and (D4) for stable and unstable atmosphere, respectively (Seinfeld and Pandis, 2006).

$$r_a = \frac{1}{\kappa u_*}(\ln(\frac{z}{z_0}) + 4.7(Rf_s - Rf_0))$$

$$r_a = \frac{1}{\kappa u_*}(\ln(\frac{z}{z_0}) + \ln(\frac{(\eta_0^2+1)(\eta_0+1)^2}{(\eta_s^2+1)(\eta_s+1)^2}) + 2(\tan^{-1}\eta_s - \tan^{-1}\eta_0)) \quad \text{(D3)}$$

ACPD
10, 18661–18730, 2010

$$\eta_0 = (1 - 15Rf_0)^{1/4}, \eta_s = (1 - 15Rf_s)^{1/4}, Rf_0 = \frac{z_0}{L}, Rf_s = \frac{z_s}{L}$$
$$\kappa = 0.4 \text{ (von Karman constant)} \quad \text{(D4)}$$

z_0 is the roughness length and u_* is the friction velocity. The surface layer height (z_s) can be approximated as one tenth of the total mixing height (Seibert et al., 1997). Rf_0 is the non-dimensional flux Richardson number at the roughness length scale height (z_0) and Rf_s is the flux Richardson number at the surface layer height. If Rf is larger than zero, the atmosphere is stable and Eq. (D3) is used, and if Rf is smaller than zero, the atmosphere is unstable Eq. (D4) is used instead.

The quasi-laminar resistance is calculated with Eq. (D5) over land (Zhang et al., 2001; Seinfeld and Pandis, 2006) and with Eq. (D6) over ocean (Slinn and Slinn, 1980).

$$r_b = \frac{1}{3u_* R_1 (Sc^{-\gamma} + (St/(\alpha + St))^2 + 0.5(D_p/A)^2)}$$
$$R_1 = \exp\left(-St^{1/2}\right) \quad \text{(D5)}$$

$$r_b = \frac{\kappa \cdot v}{u_*^2} \frac{1}{(Sc^{-1/2} + 10^{-3/St})} \quad \text{(D6)}$$

R_1 is the fraction of particles that stick to the surface upon contact. A, α and γ are surface specific parameters given by Zhang et al., 2001 for 12 different land use categories. St is the Stokes number and Sc is the Schmidt number.

ACPD
10, 18661–18730, 2010

Appendix E

Inorganic particle salt composition

Table E1 gives the explicit scheme which is used in ADCHEM to estimate the particle salt molar composition.

Appendix F

Dry deposition velocity for gases

The dry deposition velocities for the different gases are given by Eq. (F1) (Seinfeld and Pandis, 2006).

$$v_d = \frac{1}{r_a + r_b + r_c} \tag{F1}$$

The dry deposition can be a significant loss term for acid species like HNO_3 and H_2SO_4 which has a very large effective Henry's law constant. The effective Henry's law constants used for the different species in the chemical gas phase model are taken from Table 19.4 in Seinfeld and Pandis, 2006 which is valid for a pH of about 6.5. For most of the species no effective Henry's law constant were found, then the Henry's law constants given by Table 5.4 in Sander et al., 2006 were used instead. For many of the hydrocarbon species no Henry's law constants were found at all. It was then assumed that their solubility in water is practically zero.

The aerodynamic resistance is a function of the stability of the atmosphere but is independent of whether it is gases or particles that are deposited. The aerodynamic resistances for gases as well as for particles are therefore given by Eqs. (D3) and (D4).

The quasi-laminar resistance for gases over land is described by Eq. (F2) (Seinfeld and Pandis, 2006). Equation (F3) gives the quasi-laminar resistance over ocean (Hicks

ACPD
10, 18661–18730, 2010

and Liss, 1976).

$$r_b = \frac{5Sc_i^{2/3}}{u^*} \tag{F2}$$

$$r_b = \frac{1}{\kappa u^*} \ln\left(\frac{z_0 \kappa u^*}{D}\right) \tag{F3}$$

The canopy resistance depends on the structure of the ground. For vegetated land surfaces the resistance is divided into foliar resistance and ground resistance. Canopy resistance is the sum of the foliar resistance and the ground resistance in parallel (Seinfeld and Pandis, 2006).

The foliar resistance is divided into resistance to uptake at the surface of the leaves and at the plant stomata. The stomata resistance (r_{st}) can be further divided into the stomata pore resistance (r_p) and the mesophyll resistance (r_m) which is the resistance to dissolution in the leaf interior (Seinfeld and Pandis, 2006). The stomata resistance is usually very important for the dry deposition of gases. Since stomata are only open during the day it will lead to a diurnal pattern in the dry deposition velocity, with considerably higher values during the day than during the night (Pirjola and Kulmala, 1998 and Seinfeld and Pandis, 2006).

The complete surface resistance for species i is given by Eq. (F4) (Seinfeld and Pandis, 2006 originaly from Wesely, 1989). Apart from the stomata resistance the surface resistance also depends on the outer surface resistance in the upper canopy (r_{lu}), transfer resistance by buoyant convection (r_{dc}), the resistance to uptake by leaves, twigs and other surfaces (r_{cl}) and the resistance at the ground including transfer resistance due to canopy height (r_{ac}) and resistance in the soil (r_{gs}).

$$r_c^i = \left(\frac{1}{r_{st}^i} + \frac{1}{r_{lu}^i} + \frac{1}{r_{dc}^i + r_{cl}^i} + \frac{1}{r_{ac}^i + r_{gs}^i}\right)^{-1} \tag{F4}$$

ACPD
10, 18661–18730, 2010

Appendix G

Radiative transfer model

The radiative transfer equation for solar irradiance can be written as in Eq. (G1) (Jacobson, 2005).

$$\mu \frac{dI_{\lambda,\mu,\phi}}{d\tau_\lambda} = I_{\lambda,\mu,\phi} - J^{\text{diffuse}}_{\lambda,\mu,\phi} - J^{\text{direct}}_{\lambda,\mu,\phi} \tag{G1}$$

The diffuse component is given by Eq. (G2) and the direct component by Eq. (G3).

$$J^{\text{diffuse}}_{\lambda,\mu,\phi} = \sum_k \frac{\sigma_{s,k,\lambda}}{\sigma_\lambda} \frac{1}{4\pi} \int_0^{2\pi} \int_{-1}^{1} I_{\lambda,\mu',\phi'} P_{s,k,\lambda,\mu,\mu',\phi,\phi',d\mu',d\phi'}) \tag{G2}$$

$$J^{\text{direct}}_{\lambda,\mu,\phi} = \frac{1}{4\pi} E^{-\tau_\lambda/\mu_s}_{s,\lambda} \sum_k \left(\frac{\sigma_{s,k,\lambda}}{\sigma_\lambda} P_{s,k,\lambda,\mu,-\mu_s,\phi,\phi_s}\right) \tag{G3}$$

λ is the wavelength of light, I_λ is the the spectral radiance, E_s is the solar irradiance, τ_λ is the optical depth, Θ_s is the solar zenith angle, σ is the extinction coefficient , $\sigma_s$is the scattering coefficient, μ_s=cos(Θ_s) and Φ_s gives the direction of the solar radiation, μ and Φ gives the orientation of the beam of interest, μ' and Φ' gives the direction of the diffuse radiation and P_s is the scattering phase function, which gives the angular distribution of the scattered energy.

Approximating the integral in Eq. (G2) with quadrature two-stream equations gives Eq. (G4) (Jacobson, 2005).

$$\begin{aligned} &\tfrac{1}{4\pi} \int_0^{2\pi} \int_{-1}^{1} I_{\lambda,\mu',\phi'} P_{s,k,\lambda,\mu,\mu',\phi,\phi',d\mu',d\phi'}) \\ &\approx \begin{cases} \frac{1+g_{a,k,\lambda}}{2} I\uparrow + \frac{1-g_{a,k,\lambda}}{2} I\downarrow & \text{upward} \\ \frac{1+g_{a,k,\lambda}}{2} I\downarrow + \frac{1-g_{a,k,\lambda}}{2} I\uparrow & \text{downward} \end{cases} \end{aligned} \tag{G4}$$

ACPD
10, 18661–18730, 2010

$I\uparrow$ is the upward radiance and $I\downarrow$ is the downward radiance. Combining Eqs. (G2) and (G4) gives Eq. (G5).

$$J^{\text{diffuse}}_{\lambda,\mu,\phi} \approx \begin{cases} \omega_{s,\lambda}\frac{1+g_{a,\lambda}}{2} I\uparrow + \omega_{s,\lambda}\frac{1-g_{a,\lambda}}{2} I\downarrow & \text{upward} \\ \omega_{s,\lambda}\frac{1+g_{a,\lambda}}{2} I\downarrow + \omega_{s,\lambda}\frac{1-g_{a,\lambda}}{2} I\uparrow & \text{downward} \end{cases} \quad \text{(G5)}$$

$\omega_{s,\lambda} = \frac{\sigma_{s,\lambda}}{\sigma_{\lambda}}$, is the single scattering albedo and $g_{a,\lambda}$ is the effective asymmetry parameter, calculated from the asymmetry parameters for gases ($g_{a,g,\lambda}$), particles ($g_{a,p,\lambda}$) and cloud drops ($g_{a,c,\lambda}$).

$$g_{a,\lambda} = \frac{\sigma_{s,a,\lambda} g_{a,p,\lambda} + \sigma_{s,c,\lambda} g_{a,c,\lambda}}{\sigma_{s,g,\lambda} + \sigma_{s,p,\lambda} + \sigma_{s,c,\lambda}} \quad \text{(G6)}$$

If using the quadrature approximation Eqs. (G4) and (G1) can be written as:

$$\begin{cases} \mu_1 \frac{dI\uparrow}{d\tau} = I\uparrow - \omega_s \frac{1+g_a}{2} I\uparrow - \omega_s \frac{1-g_a}{2} I\downarrow - \frac{\omega_s}{4\pi}(1-3g_a\mu_1\mu_s)E_s e^{-\tau/\mu_s} \\ -\mu_1 \frac{dI\downarrow}{d\tau} = I\downarrow - \omega_s \frac{1+g_a}{2} I\downarrow - \omega_s \frac{1-g_a}{2} I\uparrow - \frac{\omega_s}{4\pi}(1+3g_a\mu_1\mu_s)E_s e^{-\tau/\mu_s} \end{cases} \quad \text{(G7)}$$

μ_1 is equal to $1/\sqrt{3}$ when using the quadrature approximation. The spectral radiation terms in Eq. (G7) can be replaced with the spectral irradiance using the conversion:

$$E\uparrow = 2\pi\mu_1 I\uparrow, \quad E\downarrow = 2\pi\mu_1 I\downarrow \quad \text{(G8)}$$

This gives Eq. (G9) (Jacobson, 2005):

$$\begin{cases} \frac{dE\uparrow}{d\tau} = \gamma_1 E\uparrow - \gamma_2 E\downarrow - \gamma_3 \omega_s E_s e^{-\tau/\mu_s} \\ \frac{dE\downarrow}{d\tau} = -\gamma_1 E\downarrow + \gamma_2 E\uparrow + (1-\gamma_3)\omega_s E_s e^{-\tau/\mu_s} \end{cases} \quad \text{(G9)}$$

Where

$$\gamma_1 = \frac{1-\omega_s(1+g_a)/2}{\mu_1}, \quad \gamma_2 = \frac{\omega_s(1-g_a)}{2\mu_1}, \quad \gamma_3 = \frac{1-3g_a\mu_1\mu_s}{2}$$

ACPD
10, 18661–18730, 2010

Eq. (G9) is discretized and solved according to the numerically stable scheme developed by Toon et al., 1989.

Combining the direct and the diffuse spectral radiance gives the net spectral radiation:

$$I_{\text{net}}(\tau_n) = I\uparrow(\tau_n) - I\downarrow(\tau_n) - I_{dir}(\tau_n) \quad \text{(G10)}$$

Multiplying the net spectral radiance with 4π gives the spectral actinic flux in $\mathrm{W\,m^{-2}\,nm^{-1}}$.

Tabel 4.2 in Seinfeld and Pandis, 2006 originally from Fröhlich and London, 1986 gives the solar spectral irradiance at the top of the atmosphere (E_{top}), normalized to a solar constant (S) of $1367\,\mathrm{W\,m^{-2}}$. Since this spectral irradiance is independent of the composition of the atmosphere, it can be used together with a radiative transfer model to predict the actinic flux at different altitudes in the atmosphere.

The solar zenith angle (Φ_z) is calculated with Eq. (G11) (Stull, 2000).

$$\begin{aligned} \sin(\phi_z) &= \sin(\psi)\sin(\delta_s) - \cos(\psi)\cos(\delta_s)\cos\left[\frac{360 t_{\text{UTC}}}{t_d} - \lambda_e\right] \\ \delta_s &= 23.45\cos\left[\frac{360(d-173)}{365}\right] \end{aligned} \quad \text{(G11)}$$

δ_s is the solar declination angle, ψ is the latitude and λ_e is the longitude.

Supplementary material related to this article is available online at: http://www.atmos-chem-phys-discuss.net/10/18661/2010/acpd-10-18661-2010-supplement.pdf.

Acknowledgements. This work has been supported by the European Commission 6th Framework program projects: EUCAARI, contract no 036833-2 (EUCAARI) and EUSAAR, contract no 026140 (EUSAAR). We also gratefully acknowledge the support by the Swedish Research Council through project no 2007–4619 and the Strategic Research Program MERGE: Modeling the Regional and Global Earth System. The Swedish Research Council also funded

ACPD
10, 18661–18730, 2010

the purchase of the HR-ToF-AMS instrument through Research Equipment Grant no 2006–5940. The DMPS measurements at Vavihill were supported by the Swedish Environmental Protection Agency within the Swedish Environmental Monitoring Program. The support by the Swedish Research Council for Environment, Agricultural Sciences and Spatial Planning (Formas) through project no 2009–615 is also gratefully acknowledged.

The authors would also like to thank Henrik Nilsson and Susanna Gustafsson at Environmental Dept., City of Malmö for the gas and meteorological measurements in Malmö and the gas and PM emission data for Southern Sweden, Emilie Stroh at the Dept. of Epidemiology and environmental medicine at Lund University for help with the implementation of the Southern Sweden emission data and Matthias Ketzel and Fenjuan Wang from Danish National Environmental Research Institute for help with the Danish anthropogenic gas and particle emissions.

References

Arneth, A., Niinemets, Ü., Pressley, S., Bäck, J., Hari, P., Karl, T., Noe, S., Prentice, I. C., Serça, D., Hickler, T., Wolf, A., and Smith, B.: Process-based estimates of terrestrial ecosystem isoprene emissions: incorporating the effects of a direct CO2-isoprene interaction, Atmos. Chem. Phys., 7, 31–53, doi:10.5194/acp-7-31-2007, 2007.

Arneth, A., Schurgers, G, Hickler, T, and Miller, P. A.: Effects of species composition, land surface cover, CO_2 concentration and climate on isoprene emissions from European forests, Plant Biol., 10, 150–162, doi:110.1055/s-2007-965247, 2008.

Atkinson, R. and Arey, J.: Gas-phase tropospheric chemistry of biogenic volatile organic compounds: a review, Atmos. Environ., 37, 197–219, 2003.

Atkinson, R., Baulch, D. L., Cox, R. A., Crowley, J. N., Hampson, R. F., Hynes, R. G., Jenkin, M. E., Rossi, M. J., and Troe, J.: Evaluated kinetic and photochemical data for atmospheric chemistry: Volume I – gas phase reactions of O_x, HO_x, NO_x and SO_x species, Atmos. Chem. Phys., 4, 1461–1738, doi:10.5194/acp-4-1461-2004, 2004.

Atkinson, R.: Gas-phase tropospheric chemistry of volatile organic compounds .1. Alkanes and alkenes, J. Phys. Chem. Ref. Data, 26, 215–290, 1997.

Boy, M., Hellmuth, O., Korhonen, H., Nilsson, E. D., ReVelle, D., Turnipseed, A., Arnold, F., and Kulmala, M.: MALTE - model to predict new aerosol formation in the lower troposphere, Atmos. Chem. Phys., 6, 4499–4517, doi:10.5194/acp-6-4499-2006, 2006.

Bromley, L. A.: Thermodynamic properties of strong electrolytes in aqueous solutions, AIChE J., 19, 313–320, 1973.
Businger, J. A. and Arya, S. P. S.: Height of the mixed layer in the stably stratified planetary boundary layer, Advances in Geophysics, 18A, 73–92, 1974.
Calvert, J. G., Atkinson, R., Becker, K. H., Kamens, R. M., Seinfeld, J.H., Wallington, T. J., and Yarwoord, G.: The Mechanisms of Atmospheric Oxidation of Aromatic Hydrocarbons, Oxford University Press, New York, USA, 556 pp., 2002.
Clement, F. C., Kulmala, M., and Vesala, T.: Theoretical consideration on sticking probabilities, J. Aerosol Sci., 27, 6, 869–882, 1996.
Cotte, H., Devaux, C., and Carlier, P.: Transformation of Irradiance Measurements into Spectral Actinic Flux for Photolysis Rates Determination, J. Atmos. Chem., 26, 1–28, 1997.
Donahue, N. M., Robinson, A. L., Stanier, C. O., Pandis, S. N., Coupled partitioning, dilution, and chemical aging of semivolatile organics, Envir. Sci. Tech. Lib., 40, 2635–2643, 2006.
Draxler, R.R. and Rolph, G.D.: HYSPLIT (Hybrid Single-Particle Lagrangian Integrated Trajectory) Model access via NOAA ARL READY Wedsite (http://www.arl.noaa.gov/ready/hysplit4.html), NOAA Air Resources Laboratory, Silver Spring, MD, 2003.
Fitzgerald, J. W., Hoppel, W. A., and Gelbard, G.: A one-dimensional sectional model to simulate multicomponent aerosol dynamics in the marine boundary layer 1. Model description, J. Geophys. Res., 103, 16085–16102, 1998.
Fröhlich, C. and London, J. (Eds.): Revised Instruction Manual on Radiation Instruments and Measurements, World Climate Research Program (WCRP) Publication Series 7, World Meteorological Organization/TD No. 149, Geneva, 1986.
Grieshop, A. P, Miracolo, M. A., Donahue, N. M., and Robinson, A. L.: Constraning the Volatility Distribution and Gas-Particle Partitioning of Combustion Aerosols Using Isothermal Dilution and Thermodenuder Measurements, Environ. Sci. Technol., 43, 4750–4756.
Griffin, R. J., Cocker III, D. R., Flagan, R. C., and Seinfeld, J. H.: Organic aerosol formation from the oxidation of biogenic hydrocarbons, J. Geophys. Res., 107(D3), 3555–3567, 1999.
Guenther, A.: Seasonal and Spatial Variations in Natural Volatile Organic Compound Emissions, Ecol. Appl., 7(1), 34–45, 1997.
Gustafsson, S.: Uppbyggnad och validering av emissionsdatabasavseende luftföroreningar för Skåne med basår. Licentiat Dissertation at National Environmental Research Institute, Lund University, nr 9, 2001.
Haylock, M. R., Hofstra, N., Klein Tank, A. M. G., Klok, E. J., Jones, P.D. and New, M.: A

ACPD
10, 18661–18730, 2010

European daily high-resolution gridded dataset of surface temperature and precipitation for 1950–2006, J. Geophys. Res., 2008, 113, D20119, doi:10.1029/2008JD010201, 2008.
Henze, D. K. and Seinfeld, J. H.: Global secondary organic aerosol from isoprene oxidation, Geophys. Res. Lett., 33, L09812, doi:10.1029/2006GL025976, 2006.
Henze, D. K., Seinfeld, J. H., Ng, N. L., Kroll, J. H., Fu, T.-M., Jacob, D. J., and Heald, C. L.: Global modeling of secondary organic aerosol formation from aromatic hydrocarbons: high- vs. low-yield pathways, Atmos. Chem. Phys., 8, 2405–2420, doi:10.5194/acp-8-2405-2008, 2008.
Hicks, B. B. and Liss, P. S.: Transfer of SO_2 and other reactive gases across the air-sea interface, Tellus, 28, 348–354, 1976.
Iserles, A.: A First Course in the Numerical Analysis of Differential Equations. Cambridge University Press, Cambridge, United Kingdom and New York, NY, USA. ISBN:0 521 55376 8, 2004.
Jacobson, M. Z.: Numerical techniques to solve condensational and dissolutional growth equations when growth is coupled to reversible aqueous reactions, Aerosol Sci. Technol., 27, 491–498, 1997.
Jacobson, M. Z.: A Solution to the Problem of Nonequilibrium Acid/Base Gas-Particle Transfer at Long Time Step, Aerosol Sci. Tech., 39, 92–103, 2005a.
Jacobson, M. Z.: Fundamentals of Atmospheric Modelling (2nd edn.), Cambridge University Press, Cambridge, United Kingdom and New York, NY, USA, ISBN:0 521 54865 9, 2005b.
Jacobson, M. Z. and Seinfeld, J. H.: Evolution of nanoparticle size and mixing state near the point of emission, Atmos. Environ., 38, 1839–1850, 2004.
Jimenez, J. L., Canagaratna, M. R., Donahue, N. M., Prevot, A. S. H., Zhang, Q., Kroll, J. H., DeCarlo, P. F., Allan, J. D., Coe, H., Ng, N. L., Aiken, A. C., Docherty, K. S., Ulbrich, I. M., Grieshop, A. P., Robinson, A. L., Duplissy, J., Smith, J. D., Wilson, K. R., Lanz, V. A., Hueglin, C., Sun, Y. L., Tian, J., Laaksonen, A., Raatikainen, T., Rautiainen, J., Vaattovaara, P., Ehn, M., Kulmala, M., Tomlinson, J. M., Collins, D. R., Cubison, M. J., Dunlea, E. J., Huffman, J. A., Onasch, T. B., Alfarra, M. R., Williams, P. I., Bower, K., Kondo, Y., Schneider, J., Drewnick, F., Borrmann, S., Weimer, S., Demerjian, K., Salcedo, D., Cottrell, L., Griffin, R., Takami, A., Miyoshi, T., Hatakeyama, S., Shimono, A., Sun, J. Y, Zhang, Y. M., Dzepina, K., Kimmel, J. R., Sueper, D., Jayne, J. T., Herndon, S. C., Trimborn, A. M., Williams, L. R., Wood, E. C., Middlebrook, A. M., Kolb, C. E., Baltensperger, U., and Worsnop, D. R., Evolution of Organic Aerosols in the Atmosphere, Science, 326, 1525–1529, 2009.

ACPD
10, 18661–18730, 2010

Korhonen, H.: Model studies on the size distribution dynamics of atmospheric aerosols. Report series in aerosol science, No 65. Finnish association for aerosol research, ISBN:952-5027-46-5, 2004a.

Korhonen, H., Lehtinen, K. E. J., and Kulmala, M.: Multicomponent aerosol dynamics model UHMA: model development and validation, Atmos. Chem. Phys., 4, 757–771, doi:10.5194/acp-4-757-2004, 2004b.

Kristensson, A. Johansson, C., Westerholm, R., Swietlicki, E., Gidhagen, L., Widequist, U., and Vesely, V.: Real-world traffic emission factors of gases and particles measured in a road tunnel in Stockholm, Sweden, Atmos. Environ., 38, 657–673, 2004.

Kristensson, A.: Aerosol Particle Sources Affecting the Swedish Air Quality at Urban and Rural Level. Doctoral Dissertation at Department of Physics, Lund University, ISBN:91-628-6573-0, 2005.

Kristensson, A., Dal Maso, M., Swietlicki, E., Hussein, T., Zhou, J., Kerminen, V.-M., and Kulmala, M.: Characterization of new particle formation events at a background site in Southern Sweden: relation to air mass history., Tellus, 60B, 330–344, 2008.

Kulmala, M., Lehtinen, K. E. J., and Laaksonen, A.: Cluster activation theory as an explanation of the linear dependence between formation rate of 3nm particles and sulphuric acid concentration, Atmos. Chem. Phys., 6, 787–793, doi:10.5194/acp-6-787-2006, 2006.

Laakso, L., Grönholm, T., Rannik, Ü., Kosmale, M., Fiedler, V., Vehkamäki, H., and Kulmala, M.: Ultrafine particle scavening coefficients calculated from 6 years field measurements, Atmos. Environ., 37, 3605–3613, 2003.

Lane, T. E., Donahue, N. M., and Pandis, N.: Simulating secondary organic aerosol formation using the volatility basis-set apporach in a chemical transport model, Atmos. Environ., 42, 7439–7451, 2008.

Moldanová, J., Fridell, E., Popovicheva, O., Demirdjian, B., Tishkova, V., Faccinetto, A., and Focsa, C.: Characterisation of particulate matter and gaseous emissions from a large ship diesel engine, Atmos. Environ., 43, 2632–2641, 2009.

Myrup, L. O. and Ranzieri, A. J.: A Consistent Scheme for Estimating Diffusivities to Be Used in Air Quality Models, Report CA-DOT-TL-7169-3-76-32, California Department of Transportation, Sacramento, 1976.

McMurry, P. H. and Friedlander, S. K.: New particle formation in the presence of an aerosol, Atmos. Environ., 13, 1635–1651, 1979.

Mårtensson, E. M., Nilsson, E. D., de Leeuw, G., Cohen, L. H., and Hansson, H.-C.: Laboratory

ACPD
10, 18661–18730, 2010

simulations and parameterization of the primary marine aerosol production, J. Geophys Res., 108(D9), 4297, doi:10.1029/2002JD002263, 2003.
Ng, N. L., Kroll, J. H., Chan, A. W. H., Chhabra, P. S., Flagan, R. C., and Seinfeld, J. H.: Secondary organic aerosol formation from m-xylene, toluene, and benzene, Atmos. Chem. Phys., 7, 3909–3922, doi:10.5194/acp-7-3909-2007, 2007.
Niinemets, Ü., Tenhusen J. D., Harley, P. C., and Steinbrecher R. A model of isoprene emissions based on energetic requirements for isoprene synthesis and leaf photosynthetic properties for *Liquidambar* and *Quercus*, Plant Cell Environ., 22, 1319–1335, 1999.
Niinemets, U., Seufert, G., Steinbrecher, R., and Tenhunen, J.: A model coupling foliar monoterpene emissions to leaf photosynthetic characteristics in Mediterranean evergreen Quercus species, New Phytol., 153, 257–275, 2002.
O'Dowd, C. D., Facchini, M. C., Cavalli, F., Ceburnis, D., Mircea, M., Decesari, S., Fuzzi, S., Yoon, J. Y. and Putaud, J.-P.: Biogenically driven organic contribution to marine aerosol, Nature, 431, 676–680, 2004.
Odum, J. R., Hoffmann, T., Bowman, F., Collins, D., Flagan, R. C., and Seinfeld, J. H.: Gas/Particle Partitioning and Secondary Organic Aerosol Yields, Environ. Sci. Technol., 30, 2580–2585, 1996.
Paasonen, P., Sihto, S.-L., Nieminen, T., Vuollekoski, H., Riipinen, I., Plass-Dülmer, C., Berresheim, H., Birmili, W., and Kulmala, M.: Connection between new particle formation and sulphuric acid at Hohenpeissenberg (Germany) including the influence of organic compounds, Boreal Environ. Res., 14, 616–629, 2009.
Petzold, A., Hasselbach, J., Lauer, P., Baumann, R., Franke, K., Gurk, C., Schlager, H., and Weingartner, E.: Experimental studies on particle emissions from cruising ship, their characteristic properties, transformation and atmospheric lifetime in the marine boundary layer, Atmos. Chem. Phys., 8, 2387–2403, doi:10.5194/acp-8-2387-2008, 2008.
Pirjola, L.: Effects of the increased UV radiation and biogenic VOC emissions on ultrafine sulphate aerosol formation, J. Aerosol Sci., 30, 355–367, 1999.
Pirjola, L. and Kulmala, M.: Modelling the formation of H_2SO_4–H_2O particles in rural, urban and marine conditions, Atmos. Res., 46, 321–347, 1998.
Pirjola, L., Tsyro, S., Tarrason, L., and Kulmala, M.: A monodisperse aerosol dynamic module, a promising candidate for use in long-range transport models: Box model tests, J. Geophys. Res., 108(D9), 4258, doi:10.1029/2002JD002867, 2003.
Pohjola, M. A., Pirjola, L., Karppinen, A., Härkönen, J., Korhonen, H., Hussein, T., Ketzel,

ACPD
10, 18661–18730, 2010

M., and Kukkonen, J.: Evaluation and modelling of the size fractionated aerosol particle number concentration measurements nearby a major road in Helsinki - Part I: Modelling results within the LIPIKA project, Atmos. Chem. Phys., 7, 4065–4080, doi:10.5194/acp-7-4065-2007, 2007.

Ramankutty, N., Evan, A. T., Monfreda, C., and Foley, J. A.: Farming the planet: 1. Geographic distribution of global agricultural lands in the year 2000, Global Biogeochem. Cy., 22, GB1003, 2008.

Robinson, A. L., Donahue, N. M., Shrivastava, M. K., Weitkamp, E. A., Sage, A. M., Grieshop, A. P., Lane, T. E., Pierce, J. R., and Pandis, S. N.: Rethinking organic aerosols: Semivolatile emissions and photochemical aging, Science, 315, 1259–1262, 2007.

Roldin, P., Swietlicki, E., Massling, A., Kristensson, A., Löndahl, J., Eriksson, A., Pagels, J., and Gustafsson, S.: Aerosol ageing in an urban plume – Implications for climate and health, Atmos. Chem. Phys. Discuss., 10, 18731-18780, doi:10.5194/acpd-10-18731-2010, 2010.

Sander, S. P., Friedl, R. R., Golden, D. M., Kurylo, M. J., Moortgat, G. K., Keller-Rudek, H., Wine, P. H., Ravishankara, A. R., Kolb, C. E., Molina, M. J., Finlayson-Pitts, B. J., Huie, R. E., and Orkin, V. L.: Chemical Kinetics and Photochemical Data for Use in Atmospheric Studies. Evaluation Number 15, NASA, 2006

Seibert, P., Beyrich, F., Gryning, S.-E., Joffre, S., Rasmussen, A., and Tercier P.: Mixing Height Determination for Dispersion Modelling, COST Action 710, Preprocessing of Meteorological Data for Dispersion Modelling, Report of Working Group 2, 1997.

Schauer, J. J., Kleeman, M. J., Cass, G. R., and Simoneit, B. R. T.: Measurement of Emissions from Air Pollution Sources. 3. C-C Organic Compounds from Fireplace Combustion of Wood, Envir. Sci. Tech. Lib., 35, 1716–1728, 2001.

Schurgers, G., Arneth, A., Holzinger, R., and Goldstein, A. H.: Process-based modelling of biogenic monoterpene emissions combining production and release from storage, Atmos. Chem. Phys., 9, 3409–3423, doi:10.5194/acp-9-3409-2009, 2009a.

Schurgers, G., Hickler, T., Miller, P. A., and Arneth, A.: European emissions of isoprene and monoterpenes from the Last Glacial Maximum to present, Biogeosciences, 6, 2779–2797, 2009b, http://www.biogeosciences.net/6/2779/2009/.

Seinfeld, J. H. and Pandis, S. N.: Atmospheric Chemistry and Physics: From Air Pollution to Climate Change, (2nd edn.), Wiley, New Jersey. ISBN:0-471-72018-6, 2006.

Sheehan, P. E. and Bowman, F. M.: Estimated Effects of Temperature on Secondary Organic

ACPD
10, 18661–18730, 2010

Aerosol concentrations, Envir. Sci. Tech., 35, 2129–2135, 2001.
Simpson, D., Fagerli, H., Jonson, J. E., Tsyro, S., Wind, P., and Tuovinen, J.-P.: Transboundary Acidification, Eutrophication and Groud Level Ozone in Europe, Part I, Unified EMEP Model Description. EMEP Status Report 2003, ISSN 0806-4520, 2003
Sitch, S., Smith, B., Prentice, I., Arneth, A., Bondeau, A., Cramer, W., Kaplan, J., Levis, S., Lucht, W., Sykes, M., Thonicke, K. and Venevsky, S.: Evaluation of ecosystem dynamics, plant geography and terrestrial carbon cycling in the LPJ Dynamic Global Vegetation Model Global Change Biology, 9, 161–185, 2003
Slinn, S. A. and Slinn, W. G. N.: Predictions for particle deposition on natural waters, Atmos. Environ., 14, 1013–1016, 1980.
Slinn, W. G. N.: Predictions for particle deposition to vegetation canopies, Atmos. Environ., 16, 1785–1794, 1982.
Smith, B., Prentice, I. C., and Sykes, M. T.: Representation of vegetation dynamics in the modeling of terrestrial ecosystems: comparing two contrasting approaches within European climate space, Global Ecol. Biogeogr., 10, 621–637, 2001.
Steinbrecher, R., Smiatek, G., Köble, R., Seufert, G., Theloke, J., Hauff, K., Ciccioli, P., Vautard, R., and Curci, G.: Intra- and inter-annual variability of VOC emissions from natural and semi-natural vegetation in Europe and neighbouring countries, Atmos. Environ., 43, 1380–1391, 2009.
Stokes, R. H. and Robinson, R. A.: Interactions in Aqueous Nonelectrolyte Solutions. I. Solute-Solvent Equilibrium, J. Phys. Chem., 70, 2126–2131, 1966.
Stull, R. B.: Meteorology for Scientists and Engineers, (2nd edn.), ISBN:0-534-37214-7, 2000.
Shrivastava, M. K., Lane, T. E., Donahue, N. M., Pandis, S. N., and Robinson, A. L.: Effects of gas particle partitioning and aging of primary emissions on urban and regional organic aerosol concentrations, J. Geophys. Res., 113, D18301, doi:10.1029/2007JD009735, 2008.
Svendby, T. M., Lazaridis, M., and Tørseth, K.: Temperature dependent secondary organic aerosol formation from terpenes and aromatics, J. Atmos. Chem., 59, 25–46, 2008.
Tarrasón, L., Turner, S., and Fløisand, I.: Estimation of seasonal dimethyl sulphide fluxes over the North Atlantic Ocean and their contribution to European pollution levels, J. Geophys. Res., 100, 11623–11639, 1995.
Tirabassi, T. and Rizza, U.: Boundary Layer Parameterization for a Non-Gaussian Puff Model, J. Appl Meteorol., 36, 1031–1037, 1997.
Toon, O. B., McKay, C. P., Ackerman, T. P., and Santhanam, K.: Rapid Calculation of Ra-

ACPD
10, 18661–18730, 2010

diative Heating Rates and Photodissociation Rates in Inhomogeneous Multiple Scattering Atmospheres, J. Geophys. Res., 94, 16287–16301, 1989.

Tsimpidi, A. P., Karydis, V. A., Zavala, M., Lei, W., Molina, L., Ulbrich, I. M., Jimenez, J. L., and Pandis, S. N.: Evaluation of the volatility basis-set approach for the simulation of organic aerosol formation in the Mexico City metropolitan area, Atmos. Chem. Phys., 10, 525–546, doi:10.5194/acp-10-525-2010, 2010.

Tunved, P., Ström, J., and Hansson, H.-C.: An investigation of processes controlling the evolution of the boundary layer aerosol size distribution properties at the Swedish background station Aspvreten, Atmos. Chem. Phys., 4, 2581–2592, doi:10.5194/acp-4-2581-2004, 2004.

Vestreng, V., Rigler, E., Adams, M., Kindbom, K., Pacyna, J. M., van der Gon, D., Reis, H. S., and Traynikov, O.: Inventory review 2006, Emission data reported to LRTAP and NEC Directive, Stage 1, 2 and 3 review and Evaluation of Inventories of HM and POPs. EMEP/MSC-W Technical Report 1/2006 ISSN 1504-6179, available at: http://www.emep.int/, 2006.

Wesely, M. L.: Parameterization of surface resistance to gaseous dry deposition in regional-scale, numerical models, Atmos. Environ., 23, 1293–1304, 1989.

Wexler, A. S. and Clegg, S. L.: Atmospheric aerosol models for systems including the ions H^+, NH_4^+, Na^+, SO_4^{2-}, NO_3^-, Cl^-, Br^-, and H_2O. Journal of Geophysical Research, 107(D14), 4207, doi:10.1029/2001JD000451, 2002.

Wexler, A. S. and Seinfeld, J. H.: The distribution of ammonium salts among a size and composition dispersed aerosol, Atmos. Environ., 24, 1231–1246, 1990.

Zaveri, R. A., Easter, R. C., Fast, J. D., and Peters, L. K.: Model for Simulating Aerosol Interactions and Chemistry (MOSAIC), J. Geophys. Res., 113, D13204, doi:10.1029/2007JD008782, 2008.

Zhang, L., Gong, S., Padro, J., and Barrie, L.: A size-segregated particle dry deposition scheme for an atmospheric aerosol module, Atmos. Environ., 35, 549–560, 2001.

Zhang, K. M. and Wexler, A. S.: Modeling urban and regional aerosols-Development of the UCD Aerosol Module and implementation in CMAQ model, Atmos. Environ., 42, 3166–3178, 2008.

ACPD
10, 18661–18730, 2010

Table E1. Explicit scheme used to estimate the particle salt molar composition.

Salt	if $n_{S(VI)} > n_{NH_4} + n_{Na}$	if $n_{S(VI)} < n_{NH_4} + n_{Na}$ & $n_{S(VI)} + n_{NO_3} > n_{NH_4} + n_{Na}$	if $n_{S(VI)} + n_{NO_3} \leq n_{NH_4} + n_{Na}$ & $2n_{S(VI)} + n_{NO_3} > n_{NH_4} + n_{Na}$	if $2n_{S(VI)} + n_{NO_3} \leq n_{NH_4} + n_{Na}$
$(Na)_2SO_4$	0	0	$n_{Na} - n_{Cl}$	$n_{Na} - n_{Cl}$
$NaHSO_4$	$n_{Na} - n_{Cl}$	$n_{Na} - n_{Cl}$	0	0
NaCl	n_{Cl}	n_{Cl}	n_{Cl}	n_{Cl}
$(NH_4)_2SO_4$	0	0	$n_{NH_4} + n_{Na} - n_{NO_3} - n_{S(VI)} - n_{(Na)_2SO_4}$	$n_{S(VI)} - n_{(Na)_2SO_4}$
NH_4HSO_4	n_{NH_4}	$n_{S(VI)} - n_{NaHSO_4}$	$n_{S(VI)} - n_{(NH_4)_2SO_4}$	0
H_2SO_4	$n_{S(VI)} - n_{NH_4} - n_{NaHSO_4}$	0	0	0
NH_4NO_3	0	$n_{NH_4} - n_{NH_4HSO_4}$	n_{NO_3}	n_{NO_3}
HNO_3	n_{NO_3}	$n_{NO_3} - n_{NH_4NO_3}$	0	0
NH_3	0	0	0	$n_{NH_4} - n_{NO_3} - 2n_{(NH_4)_2SO_4}$

ACPD
10, 18661–18730, 2010

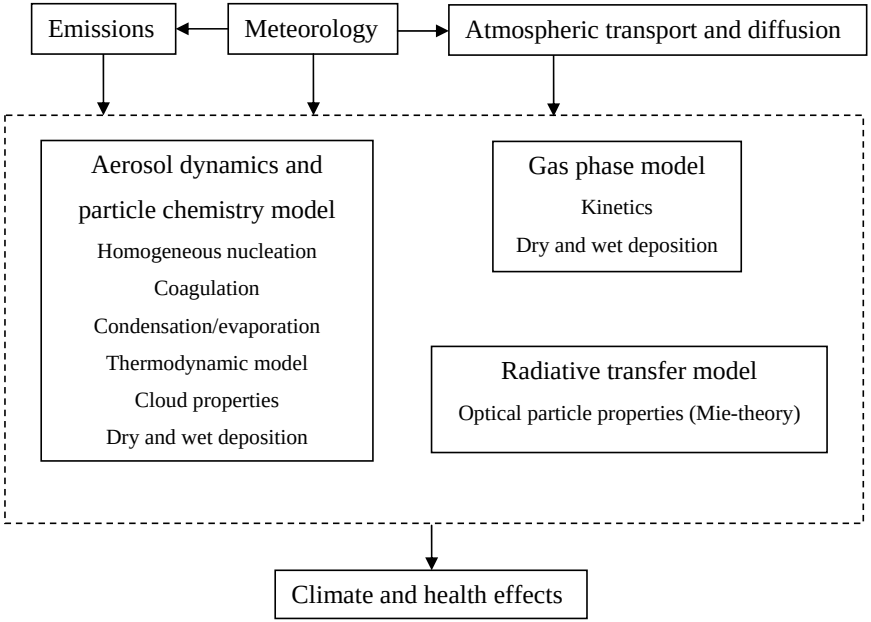

Fig. 1. Schematic picture illustrating the model structure of ADCHEM.

ACPD
10, 18661–18730, 2010

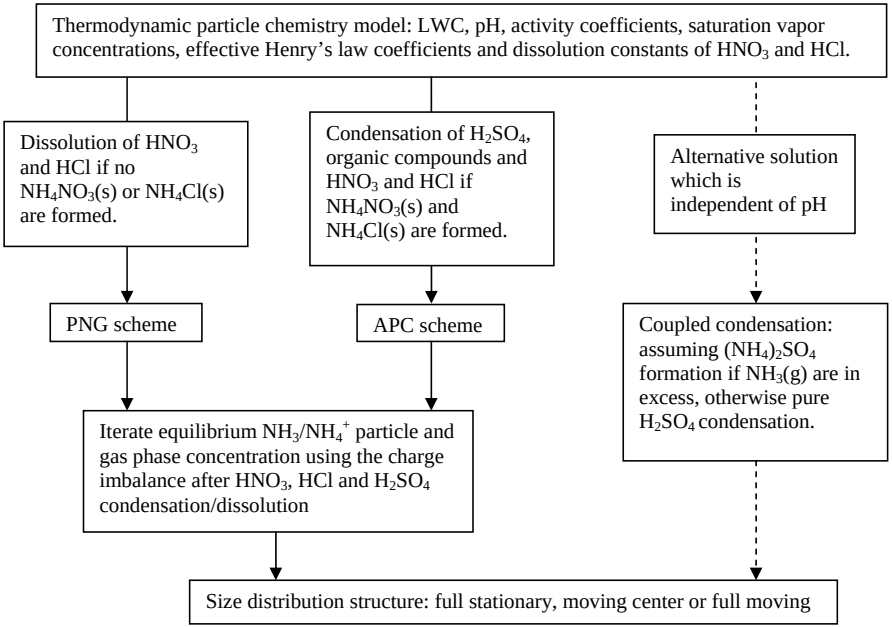

Fig. 2. Schematic picture illustrating the condensation module used in ADCHEM.

ACPD
10, 18661–18730, 2010

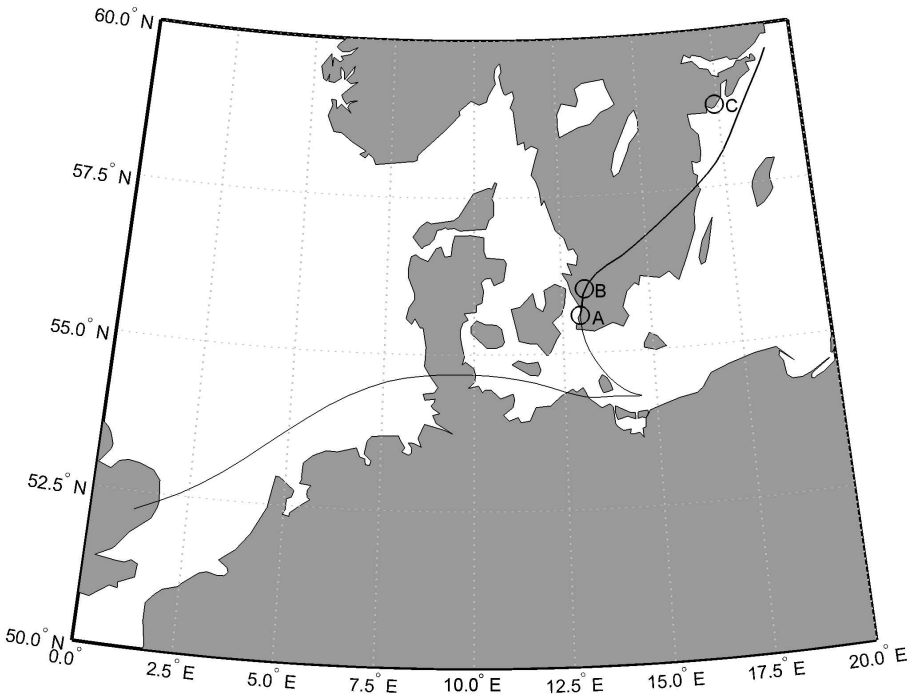

Fig. 3. Map with the air mass trajectory from the HYSPLIT model, used when modeling the urban plume from Malmö. The trajectory starts over England 48 h upwind Malmö. It arrives in Malmö 100 m a.g.l. on 21 June, 2006, at 06:00 a.m. After Malmö (A) the trajectory moves northward over Sweden. About 3 h downwind Malmö the trajectory reach Vavihill (B) and 18 h downwind Malmö it passes near the background station Aspvreten (C).

ACPD
10, 18661–18730, 2010

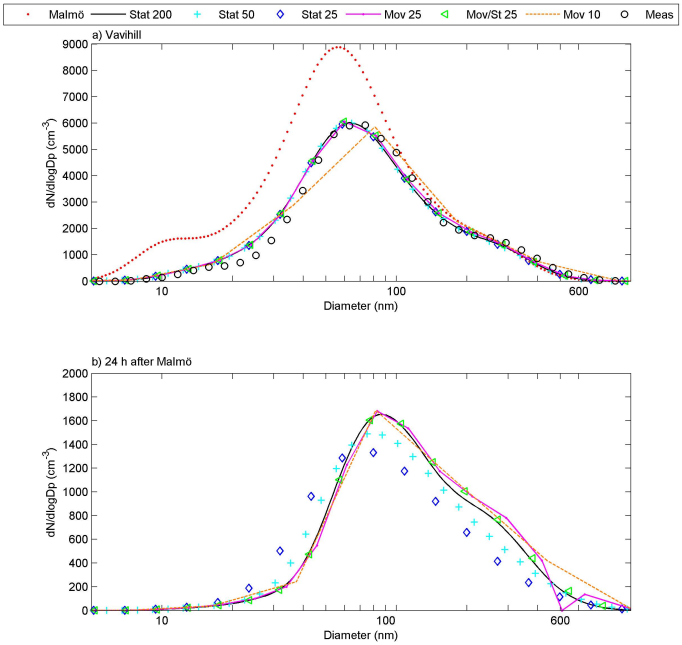

Fig. 4. Modeled particle number size distributions in the center of the urban plume at Vavihill **(a)** and 24 h downwind Malmö **(b)**, using with different size structure methods. The results are from the simulations with the full-stationary structure using 200, 50 or 25 size bins, moving-center structure with 25 or 10 size bins and a combination of the moving-center method and full-stationary method using 25 size bins (Mov/St). (a) also displays the modeled (fitted) particle number size distribution at the measurement station in Malmö and the measured particle number size distribution at Vavihill.

ACPD
10, 18661–18730, 2010

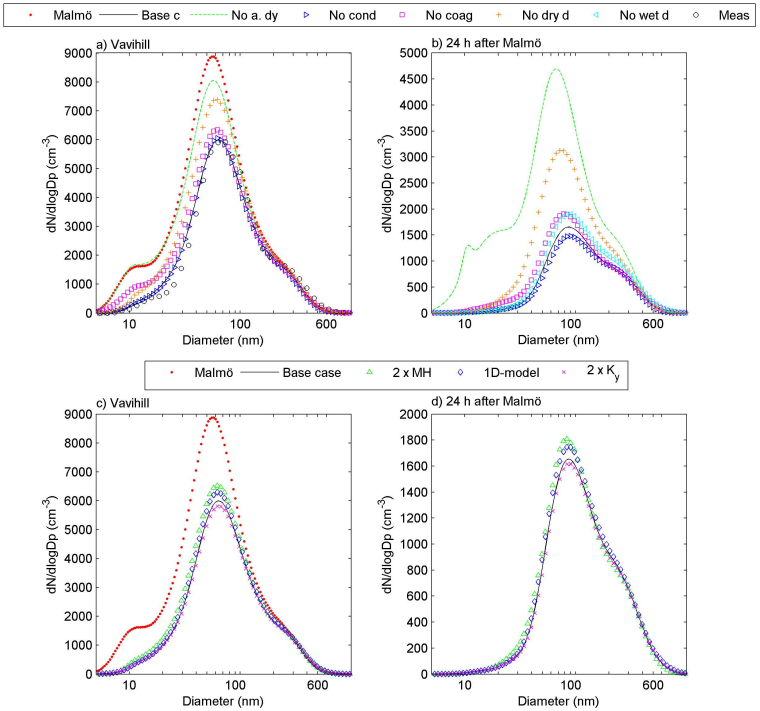

Fig. 5. Modeled particle number size distributions in the center of the urban plume at Vavihill (**a** and **c**) and 24 h downwind Malmö (**b** and **d**), without different aerosol dynamic processes (a and b) and changed vertical or horizontal mixing (c) and (d). (a) and (b) give the results from the simulations with all aerosol dynamic processes included (base case), no aerosol dynamic processes, no condensation, no coagulation, no dry deposition and no wet deposition (only in b). (c) and (d) display the results from the reference simulation, doubled mixing height (MH), no horizontal mixing (1-D-model) and doubled horizontal mixing ($2\times K_y$). In (a) the modeled (fitted) particle number size distribution at the measurement station in Malmö and the measured distribution at Vavihill is also illustrated.

ACPD
10, 18661–18730, 2010

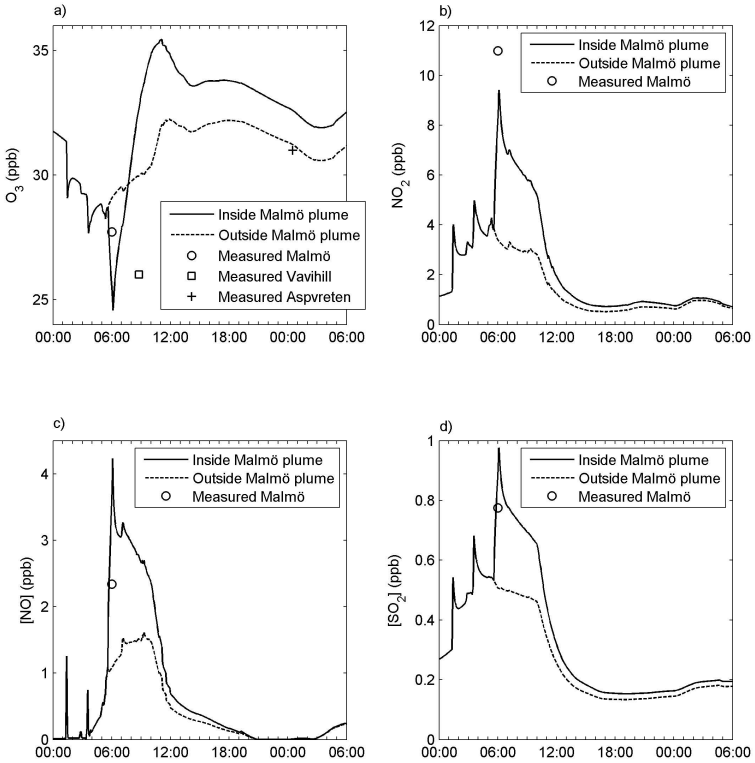

Fig. 6. Modeled concentrations of **(a)** O_3, **(b)** NO_2, **(c)** NO and **(d)** SO_2 in the surface layer, from 6 h before Malmö (00:00) to 24 h downwind Malmö (06:00), in the center of the urban plume and outside the urban plume. Given are also the measured O_3 concentrations in Malmö, at Vavihill and at Aspvreten, and the measured NO, NO_2 and SO_2 concentrations in Malmö.

ACPD
10, 18661–18730, 2010

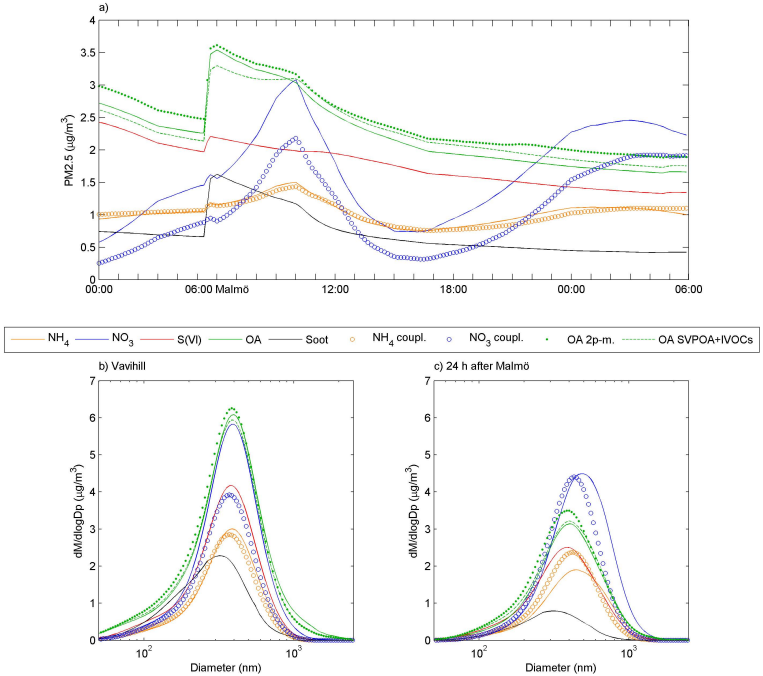

Fig. 7. **(a)** modeled $PM_{2.5}$ ammonium, nitrate, sulfate, organic aerosol (OA) and soot from 6 h before Malmö (00:00) until 24 h downwind Malmö. For ammonium and nitrate results are shown both from the uncoupled and coupled condensation simulations. For the organics the different results are from the simulation with the 2D-VBS treating POA as non-volatile and without IVOC emissions, 2D-VBS with SVPOA and IVOC emissions 1.5 times larger than the POA emissions and the 2-product model simulation. **(b)** and **(c)** gives the modeled particle mass size distributions of the different compounds at Vavihill and 24 h downwind Malmö.

ACPD
10, 18661–18730, 2010

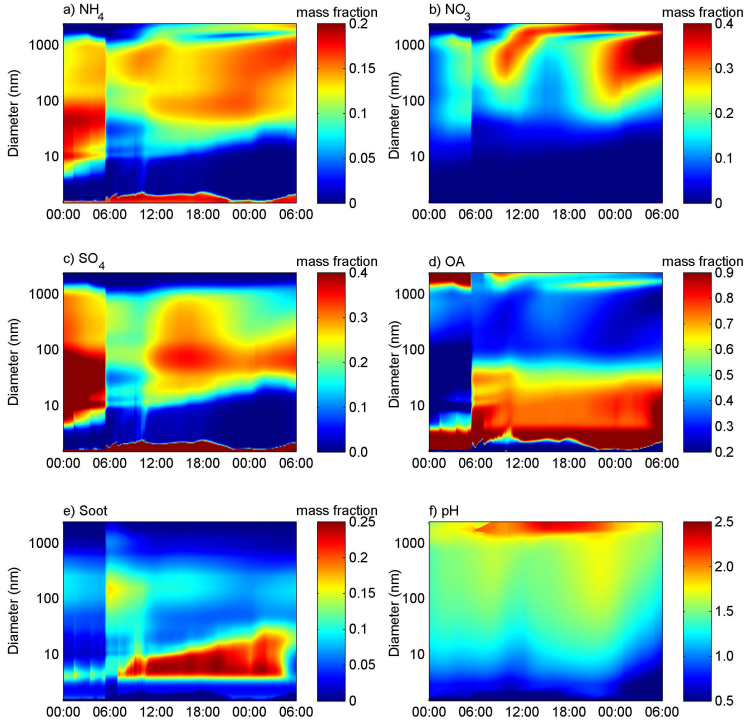

Fig. 8. Modeled size resolved particle mass fractions and pH in each size bin, starting 6 h before Malmö (00:00) and ending 24 h downwind Malmö, **(a)** for ammonium, **(b)** nitrate, **(c)** sulfate, **(d)** organic aerosol, **(e)** soot and **(f)** pH.

ACPD
10, 18661–18730, 2010

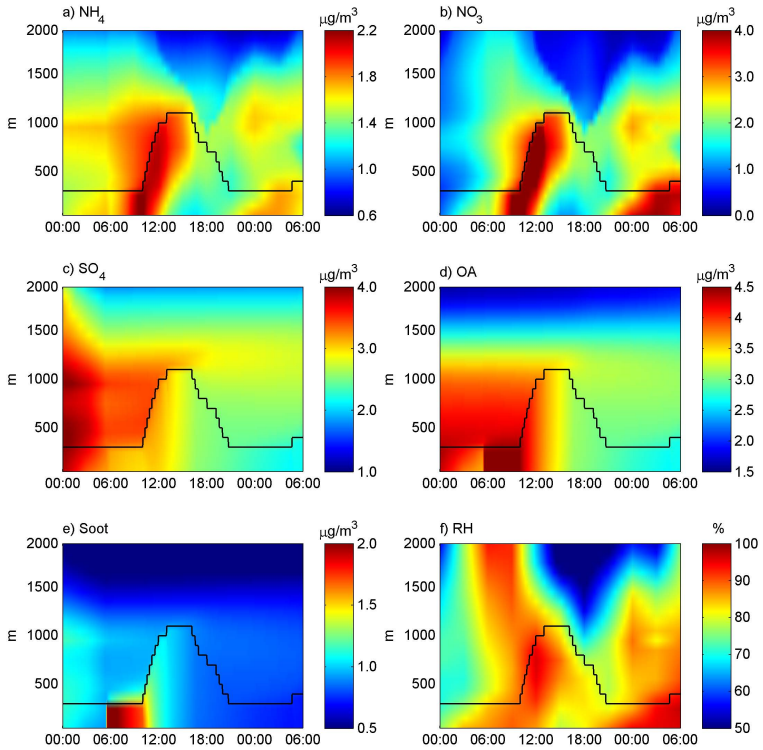

Fig. 9. Modeled $PM_{2.5}$ ammonium **(a)**, nitrate **(b)**, sulfate **(c)**, organic aerosol **(d)**, soot **(e)** and relative humidity **(f)**, from 6 h before Malmö (00:00) until 24 h downwind Malmö, in vertical direction (0–2000 m a.g.l.), in the center of the urban plume. The mixing height along the trajectory is also displayed.

ACPD
10, 18661–18730, 2010